MNRAS **000**, 1–23 (2016) Preprint 5 September 2016 Compiled using MNRAS LATEX style file v3.0

Complexes of triggered star formation in supergiant shell of Holmberg II.

Oleg V. Egorov[1⋆], Tatiana A. Lozinskaya[1], Alexei V. Moiseev[1,2], and Yuri A. Shchekinov[3]
[1] *Lomonosov Moscow State University, Sternberg Astronomical Institute, Universitetsky pr. 13, Moscow 119234, Russia*
[2] *Special Astrophysical Observatory, Russian Academy of Sciences, Nizhny Arkhyz 369167, Russia*
[3] *P. N. Lebedev Physical Institute, 53 Leninskiy Prospekt, 119991 Moscow, Russia*

arXiv:1609.00650v1 [astro-ph.GA] 2 Sep 2016

Accepted 2016 Month 00. Received 2016 Month 00; in original form 2016 Month 00

ABSTRACT

We report a detailed analysis of all regions of current star formation in the walls of the supergiant H I shell (SGS) in the galaxy Holmberg II based on observations with a scanning Fabry–Perot interferometer at the 6-m SAO RAS telescope. We compare the structure and kinematics of ionized gas with that of atomic hydrogen and with the stellar population of the SGS. Our deep Hα images and archival images taken by the *HST* demonstrate that current star formation episodes are larger and more complicated than previously thought: they represent unified star-forming complexes with sizes of several hundred pc rather than 'chains' of separate bright nebulae in the walls of the SGS. The fact that we are dealing with unified complexes is evidenced by identified faint shell-like structures of ionized and neutral gas which connect several distinct bright H II regions. Formation of such complexes is due to the feedback of stars with very inhomogeneous ambient gas in the walls of the SGS. The arguments supporting an idea about the triggering of star formation in SGS by the H I supershells collision are presented. We also found a faint ionized supershell inside the H I SGS expanding with a velocity of no greater than $10 - 15\,\mathrm{km\,s^{-1}}$. Five OB stars located inside the inner supershell are sufficient to account for its radiation, although a possibility of leakage of ionizing photons from bright H II regions is not ruled out as well.

Key words: galaxies: individual: Holmberg II – galaxies: starburst – galaxies: ISM – ISM: bubbles – ISM: kinematics and dynamics

1 INTRODUCTION

Irregular galaxies are widely used to study stellar feedback: radiation, stellar winds and supernovae that regulate the structure and kinematics of the interstellar medium (ISM) and might trigger new episodes of star formation. Due to the lack of spiral waves and the fact that gaseous discs are thicker than those in spiral galaxies, irregular galaxies reveal giant H I supershells and holes with sizes as large as 1 – 2 kpc and lifetimes up to several hundreds Myr. Giant supershells and holes in some galaxies represent the dominant feature of the ISM (see, e.g. Young & Lo 1997; Ott et al. 2001; Simpson, Hunter & Knezek 2005; Cannon et al. 2011a; Warren et al. 2011, and references therein). Such large structures are usually called supergiant shells (SGS), or giant supershells.

Formation mechanisms of supergiant shells have been discussed extensively in recent decades. In the standard approach based on the Weaver et al. (1977) model, the cumulative action of multiple stellar winds and supernovae explosions is responsible for H I shells formation (see, e.g. McCray & Kafatos 1987; Tenorio-Tagle & Bodenheimer 1988; Ott et al. 2001). However, it has been recognized long ago (see, e.g. Tenorio-Tagle & Bodenheimer 1988; Rhode et al. 1999; Kim et al. 1999; Simpson at al. 2005; Silich et al. 2006) that this scenario cannot explain the origin of giant supershells, in which the mechanical energy input from detected stellar clusters appears to be inconsistent with that required by the standard model. Several other mechanisms have been proposed: collisions of high velocity clouds with galactic discs (Tenorio-Tagle 1981), fractal ISM (Elmegreen 1997), radiation pressure from field stars (Elmegreen & Chiang 1982), ram pressure of the intergalactic medium (Bureau & Carignan 2002), H I dissolution by UV radiation (Vorobyov & Shchekinov 2004), non-linear evolution of self-gravitating turbulent galactic discs (Wada, Spaans & Kim 2000; Dib & Burkert 2005) and even exotic mechanisms (see references in Silich et al. 2006 and Warren et al. 2011).

The Im type (Magellanic-type irregulars) non-

⋆ E-mail: egorov@sai.msu.ru

© 2016 The Authors

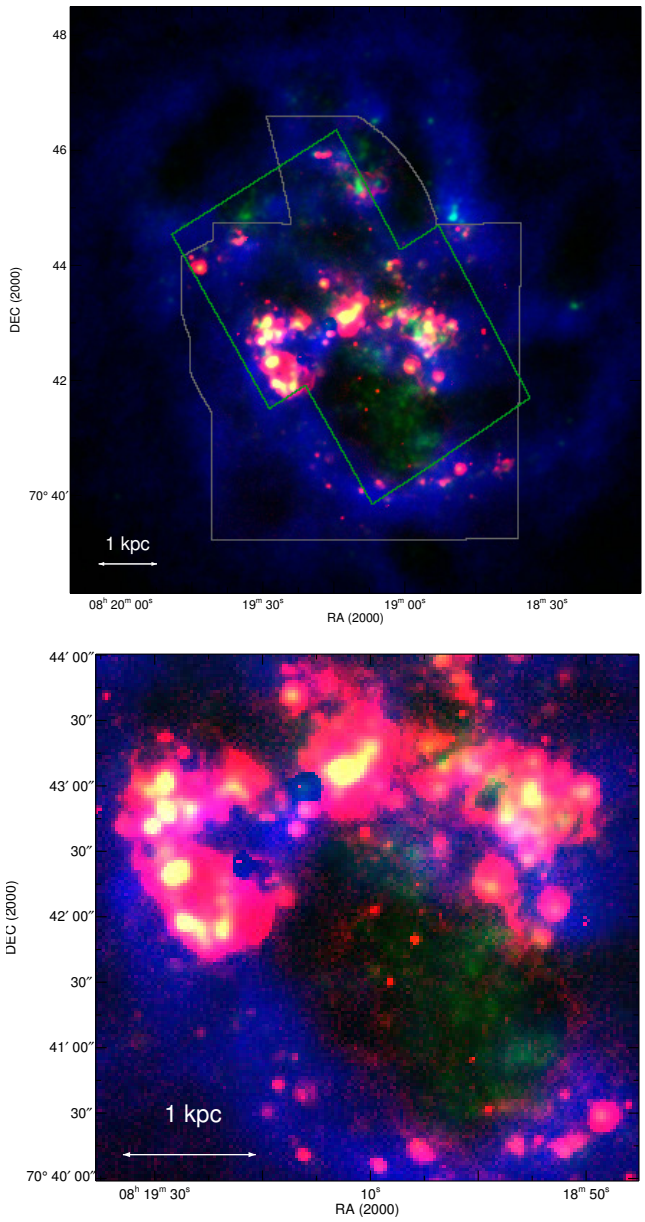

Figure 1. False-colour image of the galaxy Holmberg II: red, green, and blue channels correspond to Hα, FUV (GALEX) and H I 21 cm (LITTLE THINGS) emission, respectively. The grey line denotes the area covered by our Hα observations (both imaging and FPI) excluding the regions with optical ghosts contamination; the green line shows the area covered by *HST* data we used to identify OB-stars. Bottom image shows the area of active star formation with the different brightness setup

interacting gas-rich galaxy Holmberg II, a member of the M81 – NGC 2403 group, is one of the main 'laboratories' for studying this phenomenon. Puche et al. (1992) explained the formation of SGSs and giant H I cavities in Holmberg II by the effect of multiple supernova explosions and stellar winds of massive stars located inside the associations. Maschenko & Silich (1995) adopted this mechanism of SGSs formation and explained the discrepancy between the computed and observed elongation of many such shells by their mutual interaction and inhomogeneity of the ambient medium. The problem of the validity of such a 'standard mechanism' in the case of Holmberg II was first considered by Rhode et al. (1999) and then discussed by Bureau & Carignan (2002) and Weisz et al. (2009a). The trouble with it was that many supershells lacked young stellar associations whose energy could be sufficient to produce the observed structures.

By now, it is well established that high star-formation rates can be maintained for a much longer time period than previously believed: dwarf galaxies are characterized by the ability to sustain a high star-formation efficiency over several hundred Myr, and in some cases even up to 1 Gyr – the specific (per stellar mass unit) star formation rate is high enough to exhaust gas content in $0.4 - 1$ Gyr (McQuinn et al. 2009, 2010a,b) with local short starbursts occurring during this period. Such long periods of intense star formation provide enough energy from stellar winds and supernova explosions to drive the formation of giant cavities and supershells (see, e.g. Weisz et al. 2009b; Cannon et al. 2011a,b; Warren et al. 2011). Weisz et al. (2009a) have shown that the supershells and holes in the galaxy Holmberg II contain multiple stellar generations and might have been formed from the energy input of these stars integrated over the lifetime of the H I structure. A comparison of the energy of supergiant shells with the energy inflow from supernovae performed by Bagetakos et al. (2011) is also consistent with their formation as a result of multiple starbursts spanning a long period of time.

The energetics of supergiant shells, i.e. the fraction of energy deposited in them by supernovae explosions and stellar winds, is a crucial issue for understanding their origin. It is commonly known since the first numerical studies of dynamics of supernovae remnants Cox (1972); Chevalier (1974) that after entering the radiative expansion stage, the total energy of the remnant decreases with a radius of $\propto R^{-2}$ to $\propto R^{-3}$, so that on a time-scale of 0.1 Myr, only around 2% of the SN energy is available for driving the shell (see more recent simulations with non-equilibrium cooling by Sharma et al. 2014). Tomisaka, Habe & Ikeuchi (1981) assumed that the fraction of energy radiatively lost by a supernova might decrease, when an explosion occurs into a low density bubble produced by a stellar wind and/or previously exploded supernova(e). Within a simplistic model of sequential explosions of 20 to 100 SNe occurring at the same centre, they found qualitatively reasonable agreement with galactic superbubbles. The principal issues: the exact expansion law and the fraction of energy remained for a continuous support of growing superbubbles, have been nonetheless left beyond clear understanding. In full 3D numerical simulations of sequential SNe exploding at the same centre, Sharma et al. (2014) have found that even on a long time-scale (30 to 50 Myr), up to 30% of the injected energy can retain into slow expansion of the supershell. This conclusion is valid though only in case of 'coherent' SNe explosions, i.e. when the remnants overlap before entering the radiative stage (Nath & Shchekinov 2013). Numerical models with scattered explosions, i.e. spread through over an active volume, confirm this result: collective action of 'coherent' SNe makes them more efficient in driving supershells, with a fraction of retained energy of ~ 0.1 on times up to 10 Myr (Vasiliev, Nath & Shchekinov 2015; Yadav et al. 2016). In all cases, the expan-

sion sets asymptotically into a power law close to the standard $t^{3/5}$ wind regime with mechanical luminosity reduced by a factor of approximately 10, though still depending on interrelation between gas density and SN rate Vasiliev, Nath & Shchekinov (2015). When the origin of supergiant shells of kpc-scales are concerned, particularly in such galaxies as Ho II and IC 2574, where signs of merging of different superbubbles are clearly seen, numerical description becomes more challenging. However, in conditions typical of dwarf galaxies, the wind expansion law with energy reduced by a factor of 10 would be a reasonable conservative approach.

Short (about 10 Myr) local starbursts, which we observed as complexes of ionized gas, are located mainly inside dense walls of giant H I structures in Holmberg II. According to the modern concepts, ongoing star formation there could be triggered by the expansion and/or collision of supergiant shells. The analysis of the influence of these new sites of star formation on the evolution of supergiant shells and hence on the structure of the gaseous medium of the galaxy is of greatest interest.

This work is a third in the series of our investigations of the galaxy Holmberg II. Previously in Egorov, Lozinskaya & Moiseev (2013), we studied the ionized gas spectra of star-forming regions in Ho II using optical long-slit spectroscopic observations carried out with the 6-m SAO RAS telescope. We estimated oxygen, nitrogen, sulphur, neon and argon abundances in individual H II regions and found the average metallicity in the galaxy to be either 0.1 $Z_\odot$ or 0.3 $Z_\odot$ depending on the estimation method applied.

In Wiebe et al. (2014), we performed a multiwavelength photometric study of star formation regions in Ho II using archival data of GALEX, *Spitzer* and *Herschel* space telescopes. We have examined for the first time how the emission of star-forming regions over a wide wavelength range evolves with time. We traced the evolution of the fraction of polycyclic aromatic hydrocarbons (PAHs) and of the hot-grain properties in the galaxy.

The aim of this study is to analyse the kinematics of ionized gas in all regions of star formation and of their ambient neutral gas in the most extended 2 kpc sized supergiant shell in the galaxy. We search for shell-like structures of ionized gas that reveal signs of expansion and compare them with stellar population in star-forming regions. We also try to recognize kinematic evidences for possible supernovae shocks in the eastern chain of bright emission nebulae predicted by Tongue & Westpfahl (1995).

An analysis of gas kinematics in the rim of an H I SGS is of great interest, because it may help to find out how such giant structures change when affected by new local bursts of triggered star formation. When studying the supergiant H I shell with triggered star formation located in the Irr galaxy IC 2574 (Egorov et al. 2014), we found for the first time an inner weak diffuse emission of ionized gas in Hα and [S II] 6717,6731 lines with kinematic evidences for expansion. We showed that such an inner giant ionized supershell must have likely be formed as a result of the action of Lyman continuum photons escaping the star-forming regions on to the neutral gas in the supergiant H I shell. This is a new phenomenon hitherto unobserved in IC 2574, and the search of such inner shell-like H II structures inside H I supergiant shells in other irregular galaxies seems to be interesting. Earlier, we briefly announced the discovery of a similar giant faint ionized supershell inside the H I SGS in Holmberg II (Egorov, Lozinskaya & Moiseev 2015), which is seen on the bottom panel of Fig. 1; here we report the results of its investigation.

To avoid confusion, further we will use the SGS abbreviation to refer to the supergiant shell in Holmberg II under consideration and will use the full term 'supergiant shell' to denote the entire class of such objects.

This study is based on our observations conducted with the scanning Fabry–Perot interferometer (FPI) in Hα line and with narrow-band Hα , [S II] and [O III] filters at the 6-m telescope of the Special Astrophysical Observatory of the Russian Academy of Sciences (SAO RAS). High spatial and spectral resolutions of FPI data allows to analyze the ionized gas kinematics in superbubbles in details. A number of the studies made using this technique were published (see e.g. Lozinskaya, Moiseev & Podorvanyuk 2003; Relaño & Beckman 2005; Egorov, Lozinskaya & Moiseev 2010; Egorov et al. 2014; Camps-Farinã et al. 2015; Sánchez-Cruces et al. 2015, and references therein)

The observations and data reduction performed are described in Section 2. In Section 3, we overview the results of previous multiwavelength studies of Holmberg II. Section 4 is devoted to the search for expanding ionized and neutral shells and supershells. In Section 5, we analyse the morphology of H II complexes in the galaxy. In Section 6, we discuss the results obtained, including the nature of the faint ionized inner supershell inside the H I SGS. Section 7 summarizes the main results of this study.

2 OBSERVATIONS AND DATA REDUCTION

2.1 Optical FPI observations

The observations were carried out at the prime focus of the 6-m SAO RAS telescope using a scanning FPI mounted inside the SCORPIO-2 multi-mode focal reducer (Afanasiev & Moiseev 2011). The operating spectral range around the Hα emission line was cut by a narrow bandpass filter with a FWHM $\approx$ 14 Å bandwidth. The interferometer provides a free spectral range between the neighbouring interference orders $\Delta\lambda = 8.8$ Å with a spectral resolution (FWHM of the instrumental profile) of about 0.48 Å. During the scanning process, we have consecutively obtained 40 interferograms at different distances between the FPI plates. The log of these observations and parameters of the other data sets are given in Table 1, where T_{exp} is the exposure time; FOV – the field of view; $''/px$ – the pixel size; θ – the final angular resolution; $\delta\lambda$ and δv are the final spectral and velocity resolution.

The data reduction was performed using a software package running in the IDL environment. For a detailed description of the data reduction algorithms, see Moiseev (2002); Moiseev & Egorov (2008); Moiseev (2015). After the initial reduction, sky line subtraction, photometric and seeing corrections made using the reference stars, and wavelength calibration, the observational data were combined into data cubes, where each pixel in the field of view contains a 40-channel spectrum. The calibration wavelength was 6598.95 Å. We observed the galaxy in three overlapped fields

Table 1. Log of the observed data

Data set	Date of obs	T_{exp}, s	FOV	$''/px$	θ, $''$	sp. range	$\delta\lambda$ (δv)
FPI field #1	07/08 Feb 2010	40×150	$6.1' \times 6.1'$	0.71	1.8	8.8 Å around Hα	0.48 Å (22 km s^{-1})
FPI field #2	26/27 Apr 2011	40×240	$6.1' \times 6.1'$	0.71	1.4	8.8 Å around Hα	0.48 Å (22 km s^{-1})
FPI field #3	16/17 Dec 2014	40×160	$6.1' \times 6.1'$	0.71	1.4	8.8 Å around Hα	0.48 Å (22 km s^{-1})
FN655 image	18/19 Oct 2014	3600	$6.1' \times 6.1'$	0.36	1.9	Hα + [N II]	
FN674 image	18/19 Oct 2014	1800	$6.1' \times 6.1'$	0.36	2.0	[S II] 6717,6731 Å	
IFP502 image	02/03 Mar 2016	2400	$6.1' \times 6.1'$	0.36	1.8	[O III] 5007 Å	
FN641 image	18/19 Oct 2014	1200	$6.1' \times 6.1'$	0.36	2.0	Continuum	
FN712 image	18/19 Oct 2014	1200	$6.1' \times 6.1'$	0.36	2.0	Continuum	
SED525 image	02/03 Mar 2016	1200	$6.1' \times 6.1'$	0.36	2.0	Continuum	

(see Table 1), each field was exposed at two position angles in order to remove the parasitic ghost reflection. The regions of interest are filled less then a half of each observed field. This technique allowed us to get rid of the ghost contamination almost everywhere at the cost of reduced signal-to-noise ratio in the area of the ghosts (see details of this algorithm in Moiseev & Egorov 2008). The remaining symmetric ghosts are located in the outer regions of the total observed field. All the central regions studied in this paper are free from ghost contamination.

The data for all fields were reduced separately to obtain the wavelength cubes of the object. After the data reduction, we constructed mosaic of these three fields. We found the data for field #1 to be of poor quality (variable atmospheric conditions) compared to the data for the two other fields. That is why we included it in the mosaic only in the area of the faint inner supershell (see Section 6.3) in order to increase the signal-to-noise ratio there (the location of Field #1 coincides with that of #3).

In order to get rid of the stellar continuum emission in the data cube, we performed a zero-order background fit for each pixel at the edges of line profiles and then subtracted it. The analysis of Hα line profiles was carried out using the multi-component Voigt fitting (Moiseev & Egorov 2008).

The gas morphology and kinematics in the region of the interaction of multiple supershells are very complex and it would therefore be useful to exclude the regular component associated with the rotation of the galaxy to understand its local kinematics. We constructed a rotation model of Ho II from the H I velocity field using the tilted-ring approximation adapted to dwarf galaxy kinematics (Moiseev 2014) with initial parameters for Ho II taken from Oh et al. (2011) (we list them in Table 2) and then subtracted this model from the observed data cube. As a result, we have obtained the data cube that reflects the local motions caused by stellar feedback. In the final cube, zero velocity corresponds to the regions that show no signs of the feedback influence on the kinematics of ionized gas. We described this 'derotation' method in Egorov et al. (2014).

2.2 Narrow-band imaging

Deep optical images in the Hα , [S II] and [O III] emission lines were obtained at the 6-m telescope with the same SCORPIO-2 device using the filters FN655, FN674 and IFP502 with central wavelengths of 6559 Å, 6733 Å and 5014 Å, and FWHM = 97 Å, 60 Å and 18 Å respectively. The images taken with FN674 and IFP502 represent the [S II] 6717, 6731 Å and [O III] 5007 Å emission lines respectively. As the FWHM of the FN655 filter is broader than the separation between the Hα and [N II] emission lines, the image in this filter is contaminated by [N II] 6548, 6584 Å emission. However, given the mean I([N II])/I(Hα) ratio for H II regions in Ho II adopted from Egorov et al. (2013), we find that the contribution of the [N II] emission to total flux is less then 4 per cent.

We used the broad-band FN641, FN712 and SED525 filters centred on the continuum near the Hα , [S II] and [O III] emission lines to subtract the stellar contamination from the images obtained in the same night. Note that the subtraction was not ideal and residuals due to the stellar contribution can be seen in our final images in several areas, especially in those taken in the [S II] lines. In order to calibrate the emission-line images to energy fluxes, we observed the standard star AGK+81d266 (G191B2B in the case of [O III] observations) immediately after observing the galaxy.

2.3 Archival data used

In order to study the H I gas kinematics in the SGS, we analysed archival H I 21-cm line VLA data from the LITTLE THINGS survey (Hunter et al. 2012). We used the natural-weighted data cube and applied the same 'derotation' procedure to it as for the FPI data cube.

We trace the recent star formation distribution in Ho II by using the far UV images obtained with the GALEX space telescope as a part of the LITTLE THINGS survey.

To analyse the distribution of ionized gas, we use the data of the *HST* ACS/WFC Hα line observations carried out with the narrow-band filter F658N (program ID 10522, data are published in Hong et al 2013.) downloaded from the *Hubble* Legacy Archive[1]. While our Hα image is deeper than *HST* data, the last have better spatial resolution which is essential for understanding the internal structure of bright H II regions.

We adopted stellar photometry data from the ACS Nearby Galaxy Survey Treasury (ANGST) catalogue (Dalcanton et al. 2008) which includes the apparent magnitudes in the F606W and F814W filters for each star in the *HST* ACS/WFC field.

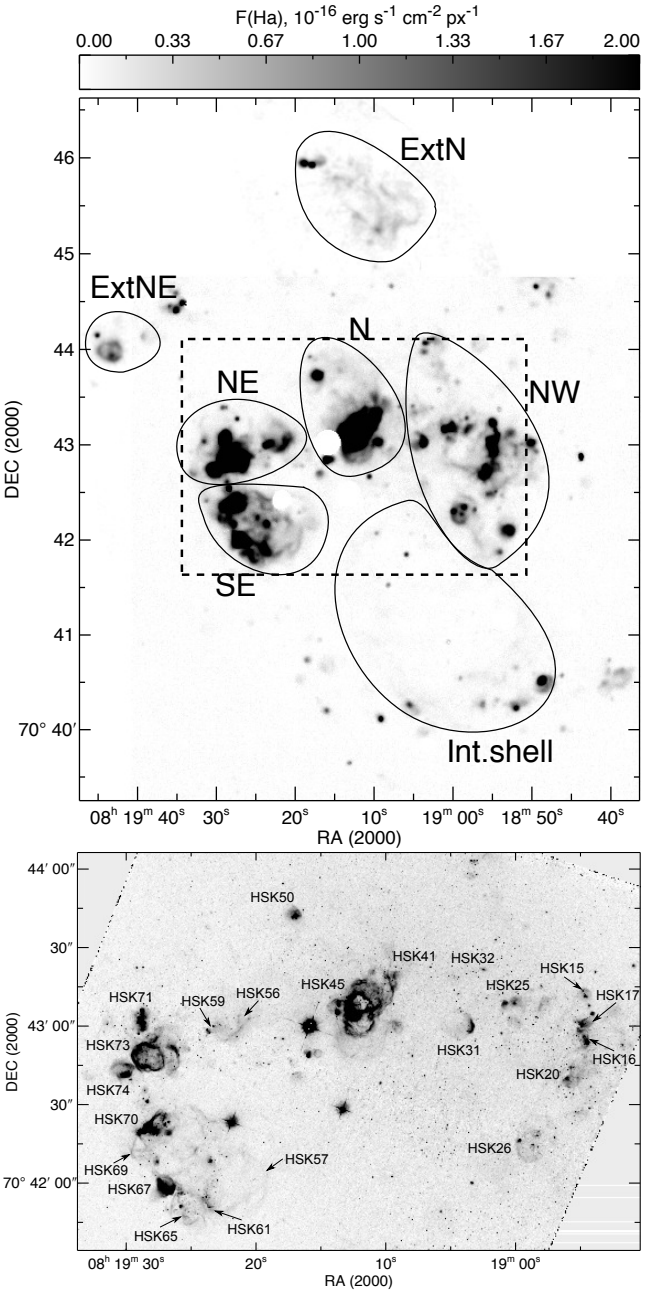

Figure 2. Top – an Hα image obtained by combining our deep narrow-band image and the sum of FPI data cube channels, with overlaid borders of the unified star formation complexes we identified (see Section 6.2) and of the internal supershell (see Section 6.3); bottom – the *HST* Hα image with HSK numbers of H II regions denoted according to Hodge et al. (1994). A dashed line on the top panel outlines the borders of the area shown on the bottom panel.

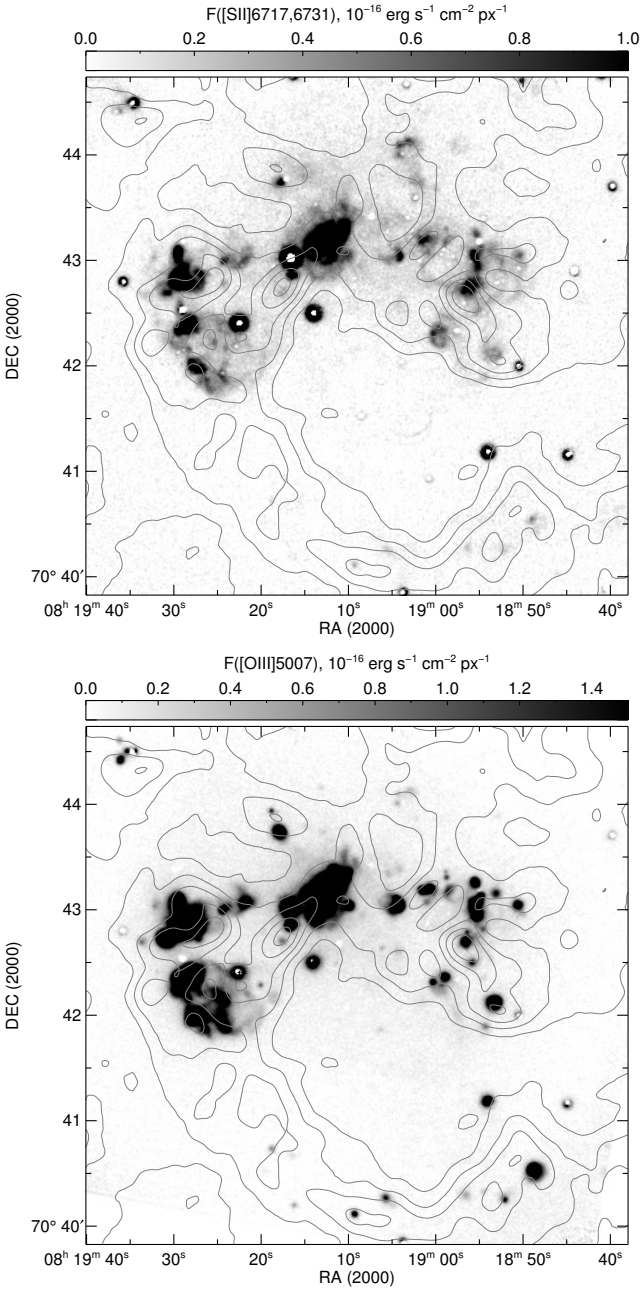

Figure 3. [S II] (top) and [O III] (bottom) images obtained with narrow-band filters after continuum subtraction. Isophotes denote the H I column density distribution.

3 MULTI-WAVELENGTH OVERVIEW OF HOLMBERG II

The galaxy Holmberg II has been thoroughly studied in the whole wavelength range. It is included in several large surveys: SINGS (Kennicutt et al. 2003), THINGS (Walter et al. 2008), LITTLE THINGS (Hunter et al. 2012), HERACLES (Leroy et al. 2009), KINGFISH (Kennicutt et al. 2011) and Local Volume galaxies database (Karachentsev, Makarov & Kaisina 2013). The basic parameters of the galaxy are listed in Table 2.

The morphology of atomic hydrogen in this galaxy is extremely inhomogeneous. The observed large-scale comet-like asymmetry of the H I disc is probably caused by the ram pressure stripping due to the hot intragroup medium (Bernard et al. 2012). The H I distribution in the galaxy

[1] http://hla.stsci.edu/

Table 2. General parameters of Holmberg II

Parameters (units)	Value
Name[a]	Holmberg II; Ho II; DDO 50; UGC 4305; PGC 23324; VII Zw 223
Centre position[b]:	
RA (J2000.0)	$08^h19^m03.7^s$
DEC (J2000.0)	$+70^\circ43'24.''6$
Morphology type[a]	Im
Holmberg radius R^c_{26}	$267.3''$ (4.4 kpc)
Distance[c]	3.39 ± 0.20 Mpc
Spatial scale	16.4 pc arcsec^{-1}
M_B magnitude[c]	-16.71 ± 0.16
Colour $B-V$[c]	0.11 ± 0.05
Gas mass[b]	1.3×10^9 $M_\odot$
Inclination	49°[b]
	38°[d]
	27°[e]
Position angle[b]	176°
Systemic velocity[b,c]	157 km s^{-1}
Rotation velocity[b]	35.7 km s^{-1}

[a]NED, NASA/IPAC Extragalactic Database (http://ned.ipac.caltech.edu/)
[b]Oh et al. (2011)
[c]Updated Local Volume galaxies database (Karachentsev et al. 2013, http://www.sao.ru/lv/lvgdb/)
[d]Moustakas et al. (2010)
[e]Sánchez-Salcedo et al. (2014)

disc represents a large number of contiguous giant supershells and 'holes' (most representable of them are shown in Fig. 1). Thus Puche et al. (1992) identified 51 giant cavities and slowly expanding H I supergiant shells in Ho II, some of which required a kinetic energy as high as 10^{53} erg for their formation. The subsequent analysis by Bagetakos et al. (2011) who used more rigid criteria allowed them to identify 39 H I cavities surrounded by shells in this galaxy, the overwhelming majority of which coincide with objects from the list by Puche et al. (1992). The sizes of shells range from 0.26 to 2.11 kpc and their expansion velocities vary in the $7-20$ km s^{-1} interval, which corresponds to the kinematic age of $10-150$ Myr.

The Ho II rotation curve determined by Puche et al. (1992) based on H I 21 cm line observations shows rigid rotation in the central region with the radius of 2 arcmin which contains the entire optical emission of the galaxy. Oh et al. (2011) performed tilted-ring analysis of the HI line-of-sight velocity field and obtained circular rotation models of the galaxy for studying the dark matter distribution. We use hereafter the basic kinematics parameters listed in Table 2 adopted from the above paper.

Note that there is still no consensus concerning the measurement of the galaxy inclination. For instance, Oh et al. (2011) reported $i = 49^\circ$; Moustakas et al. (2010) found $i = 38^\circ$ based on the results of surface photometry; Sánchez-Salcedo, Hidalgo-Gámez & Martínez-García (2014) supposed an inclination of $i \simeq 27^\circ$ requiring to place the Ho II disc above the stability threshold.

The thickness of the gaseous disk (about 400 pc) varies insignificantly with galactocentric distance (Banerjee et al. 2011), making Ho II a preferred object among other dIrr for studying the nature of supershells. Such a large vertical scale height allows supershells in Ho II to grow to large sizes before breaking through the H I disc.

Hodge, Strobel & Kennicutt (1994) identified 82 H II regions in the galaxy; hereafter for the sake of consistency we use the HSK numbers from the catalog of the above authors to denote bright H II regions shown in Fig. 2. The brightest emission nebulae are mostly concentrated in the northern wall of the most extended (about 2 kpc) H I SGS (#21 in the list by Puche et al. 1992 and #17 in the list by Bagetakos et al. 2011), which is the subject of our study. Figure 1 shows that bright H II regions form several 'chains' assembling the overall 'central arc' (this term was used by Stewart et al. 2000) in the northern wall of the SGS. The brightest of these regions are concentrated in the eastern chain. The brightest emission of heated dust is also observed in this 'central arc' (see, e.g. Hunter, Hawley & Gallagher 1993; Karachentsev & Kaisin 2007; Walter et al. 2007; Wiebe et al. 2014). In general, the location of the Hα emission agrees with the distribution of the FUV emission in the galaxy, see also figs. 5, 6 in Stewart et al. (2000) and fig. 29 in Weisz et al. (2009a). Bright regions of the FUV emission are also located in the northern rim of H I SGS. Apart from them the region of weak diffuse FUV emission extending to the southwest, three separate FUV regions to the north of the central arc and a compact one to the west of it are also seen in Fig. 1. The last one (furthest FUV region in Ho II) was analysed by Hunter, Elmegreen & Gehret (2016).

Stewart et al. (2000) studied 45 H II regions using B, Hα and FUV photometry and estimated the ages of the corresponding star-forming regions by dividing them into four age groups. Most of the star-forming regions fell into groups with ages smaller than 6.3 Myr. This is consistent with the star formation history of Ho II: according to (Weisz et al. 2008), the star-formation rate has been increasing over the last several million years.

Radio observations of the galaxy (Tongue & Westpfahl 1995; Braun et al. 2007; Heald, Braun & Edmonds 2009) revealed continuous radio emission in the region of bright emission nebulae. The above authors associated this radio emission with active star formation and suspected the presence of supernova remnants in the eastern chain of H II regions. We discuss this subject in Section 6.4 in more detail. According to the *Chandra* observatory data, the ultraluminous X-ray source (ULX) Ho II X-1 located in the eastern chain of star-forming regions is the only X-ray source in the galaxy and one of the sources of the observed bright synchrotron emission.

Earlier, the kinematics of ionized gas in Ho II was studied in detail in the neighborhood of ULX Ho II X-1 only (Lehmann et al. 2005, see also our paper Egorov, Lozinskaya & Moiseev 2016 about this object). Tomita et al. (1998) analysed the kinematics of other bright H II regions of the galaxy based on observations made with a slit spectrograph. They combined seven obtained spectra into a broad strip covering only one third of the bright H II regions in the SGS. The resulting 'position-velocity' diagrams (PV diagrams) for the H II region that the authors denoted as the 'centre' (HSK 45) revealed the radial-velocity gradient amounting to 30 km s^{-1} over 200 pc; the most blue-shifted Hα velocity is smaller than the H I velocity by about 15 km s^{-1}.

Observations of Holmberg II with FPI were performed previously at the Observatoire du mont Mégantic 1.6-m tele-

scope as a part of Hα kinematics follow-up survey of the SINGS sample (Dicaire et al. 2008). The aim of that project was to investigate the global kinematics of galaxies observed. The authors did not provide the kinematic parameters of Holmberg II due to its weak rotation and a lack of spatial coverage.

4 SEARCH FOR EXPANDING SHELLS IN STAR-FORMING REGIONS

Our deep Hα images of Holmberg II and the archival *HST* images of the galaxy (Fig. 2) reveal numerous faint extended filaments connecting several H II regions and located beyond the bright nebulae. A similar picture is observed in the [S II] and [O III] emission lines (see Fig. 3). Based on this morphology, we combined the emission features observed in the rim of the SGS into four extended areas (SE, NE, N and NW in Fig. 2) and into two areas beyond the SGS (ExtN and ExtNE).

To confirm the conclusion that the observed emission structures we identified are indeed unified physically-bound complexes of ongoing star formation, we performed a detailed analysis of the kinematics of ionized and neutral gas in these areas.

The structure and kinematics of both ionized and neutral gas in the studied H I SGS are not homogeneous. Figure 4 shows several examples of PV diagrams in the Hα and H I lines, that demonstrate how line-of-sight velocity changes with position along a chosen direction. Deviations of the line-of-sight velocity from the circular rotation model of the galaxy (zero velocity line) are clearly seen in the largest slice #1. Signs of the 'velocity ellipses' – the characteristic feature of expanding shells – are also present in this PV diagram.

Earlier, Weisz et al. (2009a) identified four local H I shells in the SGS wall with sizes of 300 − 400 pc expanding with velocities 7−15 km s^{-1}. These shells (# 8, 12, 14 and 27 in Fig. 2 of their paper) are located in the immediate vicinity of the H II HSK 70, 16, 17, and 26 regions (see fig. 2). In addition, shells # 16 and 23 are also seen and located north of the central chain of star-forming regions which might be connected with it.

We refined the location of the H I shells associated with star-forming regions and performed search for ionized gas shells in the galaxy. Below, we report the details and results of our kinematic analysis.

An expanding shell can be identified by a velocity ellipse (or a part of it) in PV diagrams or by splitting of an emission-line profile. In the case where the expansion velocity of a shell is small and spectral resolution is insufficient to resolve two components, the shell distinguishes itself by its higher velocity dispersion in the centre.

We used all the above techniques to search for expanding shells and estimate their expansion velocities.

Figure 5 shows the H I column density and line-of-sight velocity dispersion (second moment) maps for three areas – SE, N and NW – where we see increased H I velocity dispersion. The areas of high velocity dispersion in Fig. 5 correspond indeed to the expanding H I superbubbles. This suggestion is confirmed by our analysis of PV diagrams. For example, the 'velocity ellipse' might be seen at positions of

Table 3. Expansion velocity, size and kinematic age of faint shell-like structures of ionized gas shown in Figs. 7–12. Ages of the bright H II regions tied with these shells are also shown.

Shell	V_{exp}, km s^{-1}	Size, pc	Age, Myr
SE1	15	86	1.7
SE2	30–37	322 × 230	2.6
SE3	25–30	282 × 188	2.8
SE4	27–32	190 × 128	1.8
SE5	27	358 × 240	4.0
SE6	$\lesssim 20$	74	1.1
Age of HSK 67, 70:			3.8 − 4.8*
			2.5 − 4.5**
NE1	26	72 × 50	0.8
NE2	15	162 × 104	3.2
NE3	17	254 × 224	4.5
NE4	24	210 × 168	2.6
Age of HSK 59, 71, 73:			3.5 − 4.1*
			2.5 − 4.5**
N1	22	362 × 316	4.9
N2	28	142 × 96	1.5
N3	10	124 × 76	3.7
N4	18	230 × 203	7.2
Age of HSK 45:			3.7*
			2.5 − 3.5**
NW1	25	392 × 312	4.7
NW2	21	112 × 70	1.6
NW3	21	163 × 102	2.3
NW4	27	216	2.4
NW5	$\simeq 20$	226	3.4
Age of HSK 15, 16, 17, 20, 25:			4.8 − 6.2*
			4.5 − 6.3**
ExtNE1	20	49	1.5
Age of ExtNE:			3.5 − 4.5**
ExtN1	23	139	3.6
Age of ExtN:			3.5 − 4.5**
S1	40	120	1.8

*Estimates made by Wiebe et al. (2014) using Hβ equivalent width.
**Estimated by Stewart et al. (2000) using Hα and FUV data.

100 − 140 , 170 − 220 arcsec along PV diagram # 1 (HI) and 15 − 65 arcsec along PV diagram # 2 (HI) in Fig. 4, which correspond to the regions of the increased velocity dispersion in Fig. 5 in the areas of N, NW and SE respectively.

It was shown in many studies (Muñoz-Tuñón et al. 1996; Moiseev & Lozinskaya 2012, see also references therein) that the intensity – velocity dispersion diagrams of ionized gas ($I - \sigma$) can be successfully used to identify areas, where the increased velocity dispersion is caused by expanding shells. We fitted the Hα line profile to a single-component Voigt profile in each pixel obtained from the FPI data cube and constructed the $I - \sigma$ diagram for the galaxy Holmberg II (see Fig. 6). The red line in the diagram marks the intensity-weighted average velocity dispersion of ionized gas in the galaxy – $\sigma_m = 20.4 \pm 7.1$ km s^{-1}. Identical colours in the diagram (the top panel) and map (the bottom panel) are used to highlight the characteristic areas. Thus, the horizontal strip with relatively low velocity dispersion and high surface brightness marked in blue corresponds to bright H II regions and includes 50 per cent of the galaxy's Hα flux. Areas of increased dispersion, which are most likely associated with spectroscopically unresolved expanding shells, are shown in green colour, whereas the red colour corresponds to shell-like structures with clear separation of the components of the Hα line profile. The remaining areas of the increased

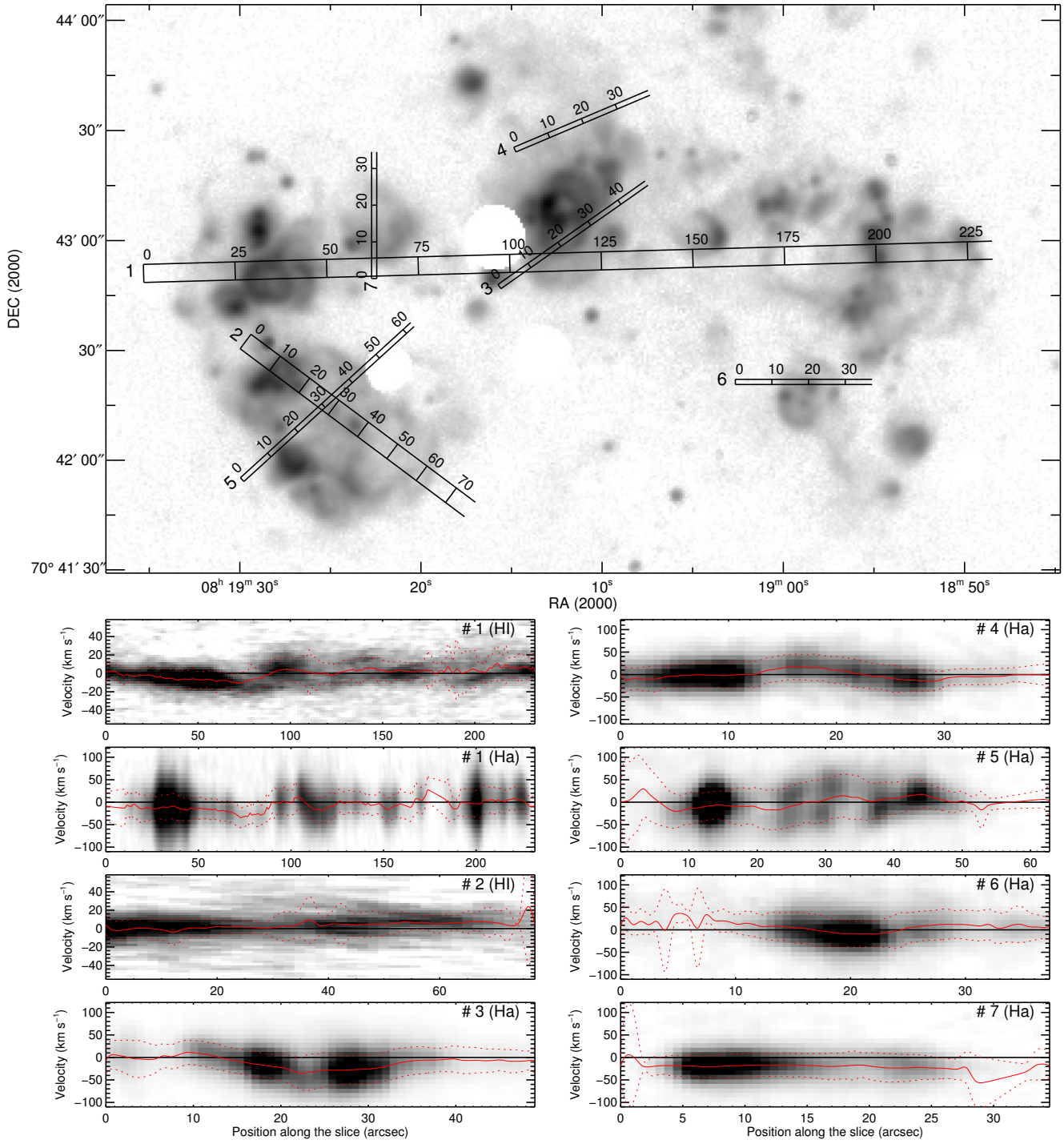

Figure 4. Examples of Hα and HI PV-diagrams. Top panel: an Hα image arcsinh (intensity-scale) with the localization of the PV diagram superimposed. PV diagram names shown to the left of the bar denote their position. Bottom panels: examples of PV diagrams with the median velocity (red solid curves) and its dispersion (red dotted curves) overlaid. The zero-velocity line is shown by a black solid line.

velocity dispersion are shown in orange colour, and areas of low surface brightness, in grey colour.

We performed a more bona fide search for expanding structures of ionized gas by analysing the PV diagrams that uniformly cover each region of ongoing star formation in the galaxy. Some examples of them are shown in Fig. 4. In the areas shown in red colour in Fig. 6, we see clear evidence for gas expansion in the form of the velocity ellipse or a part of it. Subsequent fitting of the Hα profiles by one, two or

Table 4. Sizes and ionization budget of complexes of ongoing star formation

Complex	Size pc	F(Hα), 10^{-13} erg s^{-1} cm^{-2}	N(OV5)	N(OB)	$Q_{H\alpha}$ 10^{50} s^{-1}	Q_{stars} 10^{50} s^{-1}
SE	1150 × 1050	9.3	56	35	8.8	9.7
NE	1400 × 980	9.7	58	26	9.1	8.3
N	1500 × 1000	14.0	83	36	13.2	11.1
NW	2450 × 1600	8.4	50	31	7.9	7.6
Int.shell (diff)	2730 × 2280	0.7	4	5	0.7	1.0
Int.shell (all)	2730 × 2280	1.7	10	7	1.6	1.5
ExtN	1530 × 1030	1.1	7	8*	1.1	1.9*
ExtNE	960 × 700	0.5	3	3	0.5	1.1

*Might be underestimated because of the incomplete coverage by *HST* observations (see Fig. 1).

three Voigt components allowed us to estimate the expansion velocities of the corresponding structures.

Our analysis of gas kinematics in the H I and Hα lines revealed three local neutral-gas shells associated with star-forming regions and 22 ionized gas shells. Their location is shown in grey and blue colours respectively in Fig. 7 – 12.

We found no signs of expansion of bright H II regions. Despite a rather high spectral resolution of FPI, the expansion velocities of these regions proved to be low: it does not exceed 11 km s^{-1} (half of the instrumental FWHM of FPI used). All the expanding shells of ionized gas, which we found, represent faint filamentary features in the Hα image and possibly reside in a medium with a relatively low density. In our earlier paper Wiebe et al. (2014), we have estimated the expansion velocity of the H II regions HSK45 and HSK73, however, it is now clear that the evidence of their expansion does not refer to bright nebulae but rather to faint shell-like ionized-gas structures around them.

We estimated the kinematic ages of the identified local H II shells in terms of Weaver et al. (1977) model by the following relation:

$$t = 0.6R/V_{\rm exp},$$

where R is the radius in pc, $V_{\rm exp}$ – the expansion velocity in km s^{-1} and t – the age in Myr.

To estimate the ages of bright H II regions that show no signs of its expansion, in Wiebe et al. (2014) we used the equivalent width (EW) of the H_β emission line which correlates rather well with the age of H II regions (see, e.g. Schaerer & Vacca 1998; Leitherer et al. 1999).

The derived ages of the faint local shells found inside the H II complexes and of bright H II regions are summarized in Table 3. This table also lists the age estimates made by Stewart et al. (2000) for star-forming regions based on the results of FUV and optical observations. Because of the uncertainty in the method used for age determination, the above authors divided all H II regions studied into four age groups: $0-3.5$ Myr, $3.4-4.5$ Myr, $4.5-6.3$ Myr and older than 6.3 Myr (see table 5 in their paper).

Given the results of the search for expanding shells and the study of their kinematics, we can conclude that the observed emission structures in the four areas in the SGS walls (SE, NE, N and NW) that we identified based on morphology and in two areas outside the SGS (ExtN and ExtNE) are indeed physically connected. This means (see also Sections 5 and 6.2 below) that the current star formation in the galaxy is represented by unified complexes with sizes of several hundred pc which combine several bright nebulae.

5 MORPHOLOGY AND IONIZATION BUDGET OF STAR FORMATION COMPLEXES

As shown above, the deep Hα images of the galaxy and the presence of local H I and H II shells suggest the existence of unified extended complexes joining several bright HSK nebulae. Hence the four extended areas (SE, NE, N and NW in Fig. 2) that we identified in the SGS studied and the areas outside this SGS (ExtN and ExtNE) are physically connected complexes of ongoing star formation.

Each of the star forming complexes contains several young star clusters. Weisz et al. (2009a) and Bastian et al. (2011) compared observed colour-magnitude diagrams based on *HST* data to stellar evolution tracks and selected objects younger than 10 Myr that should be OB stars. We used the same method as Weisz et al. (2009a) to obtain the list of OB stars with their magnitudes from the Hubble source catalogue (HSC[2]). The locations of the OB stars identified in such a way agree well with the list reported by Bastian et al. (2011). We used F555W- and F814W-band photometry to estimate the V-band absolute magnitude of each star. We further assume that all the selected stars are young main-sequence stars (the method used to select them should ensure this) and use O-type star models from Martins, Schaerer & Hillier (2006) to compute the bolometric luminosity and the number of ionizing photons Q_0 from each star. These stars are shown in Figs. 7–12 by asterisks with the size proportional to their luminosity. We used the above procedure to estimate the amount of ionizing quanta Q_{stars} in Table 4 from the OB stars observed in each complex.

Similar values can be readily inferred from the observed number of Hα photons. With the observed Hα flux of each complex (corrected for interstellar extinction $A_V = 0.11^m$), we estimated the equivalent number of O5V stars (N(O5V) in Table 4) and of ionizing photons Q_0 needed for gas ionization in the area with the procedure described in Osterbrock & Ferland (2006). For the case of optical thick nebulae, its Hα luminosity L(Hα) depends on Q_0 as:

$$\frac{L({\rm H}\alpha)}{h\nu_{\rm H\alpha}} \simeq \frac{\alpha^{eff}_{\rm H\alpha}}{\alpha_B} Q_0 \simeq 0.45 Q_0, \qquad (1)$$

where the Hα effective recombination coefficient $\alpha^{eff}_{\rm H\alpha} \simeq 1.17\times10^{-13}$ cm^3 s^{-1} and the total recombination coefficient of hydrogen $\alpha_B \simeq 2.59\times10^{-13}$ cm^3 s^{-1} for $T = 10\,000$ K.

[2] http://archive.stsci.edu/hst/hsc/

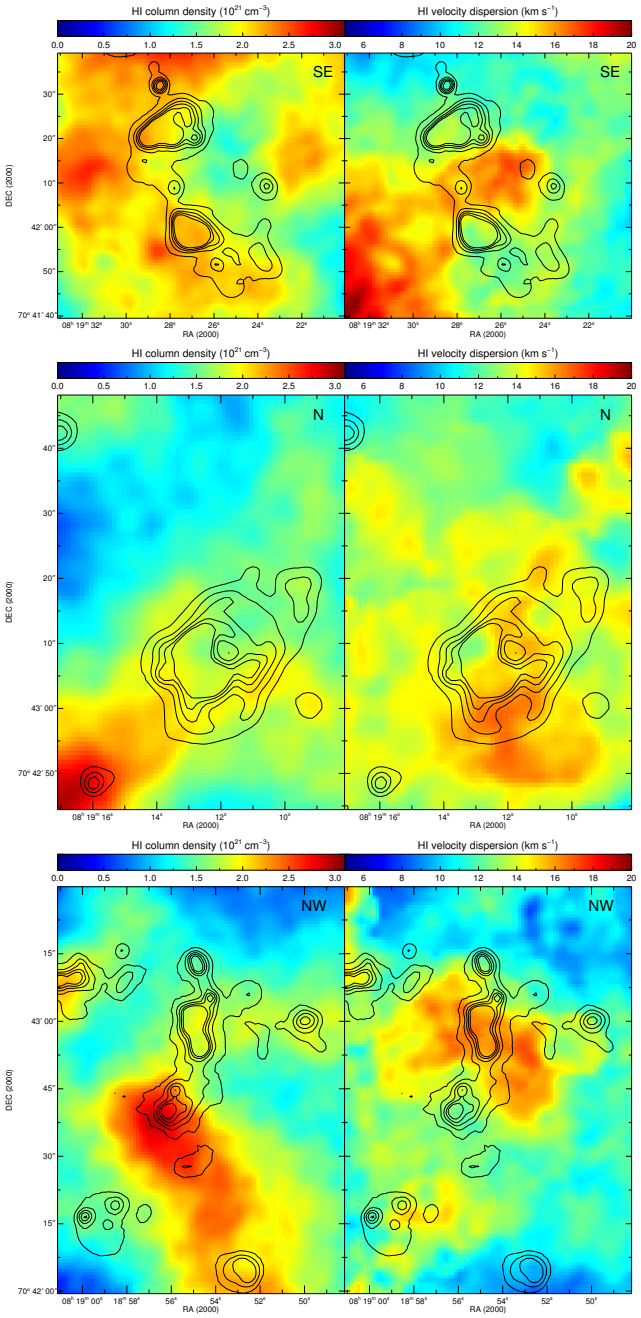

Figure 5. H I column density (left) and line-of-sight velocity dispersion (right) maps of three star-forming complexes (SE, N and NW) with local H I superbubbles detected. Hα line intensity contours are overlaid.

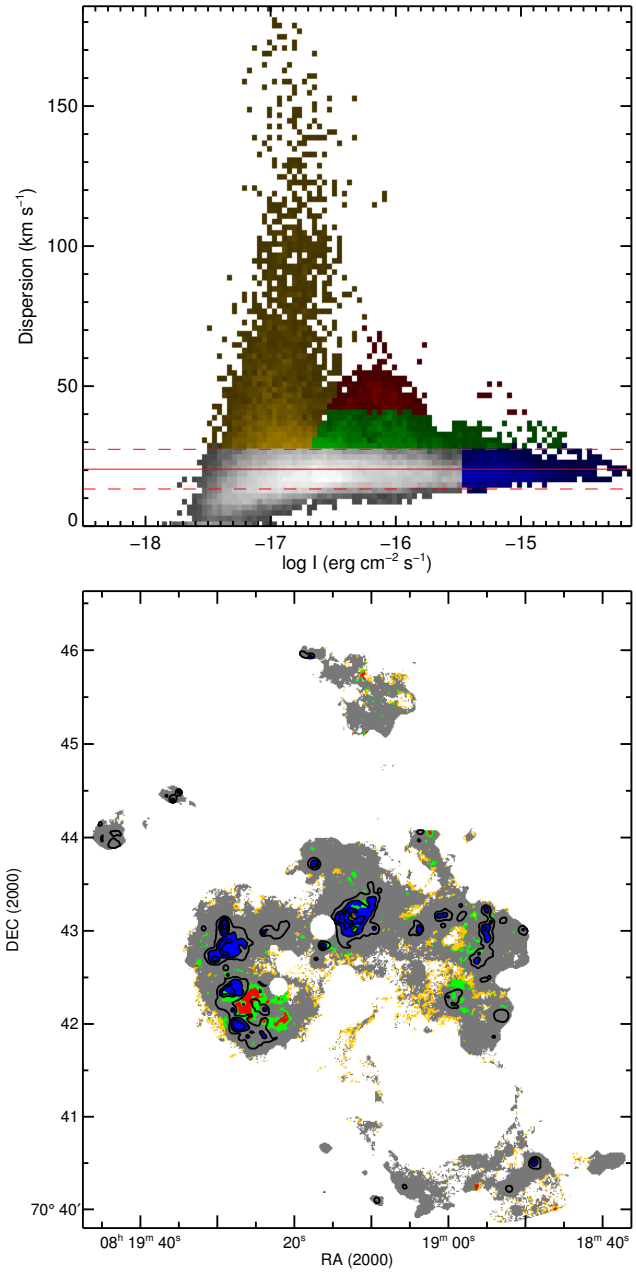

Figure 6. Hα intensity – velocity dispersion diagram for Holmberg II (top). A red solid horizontal line marks the intensity-weighted mean velocity dispersion of ionized gas in Ho II and the dashed lines – its standard deviation. The bottom plot shows the location of regions marked by different colours in the $I - \sigma$ diagram.

Further, we will refer the estimated amount of needed ionization photons Q_0 from (1) as $Q_{\mathrm{H}\alpha}$ to mention that it has been converted from the Hα luminosity.

In such a way, our measurements of the Hα flux of H II regions and of the luminosity of OB stars inside them were used to estimate both the needed and available amount of ionizing quanta in all star formation complexes studied. The results are summarized in Table 4.

Let us now consider the structure, kinematics and energy sources in each selected H II complex in more detail.

SE complex (HSK 57, 61, 65, 67, 69 and 70)

Deep Hα images of the region reveal a faint filamentary structure connecting H II regions HSK 57, 61, 65, 67, 69 and 70 (see Fig. 7). The kinematics of neutral gas shows the existence of the local H I superbubble that has a size of about 650 × 950 pc expands with the velocity of about 20 km s^{-1} and covers the whole bright part of star formation

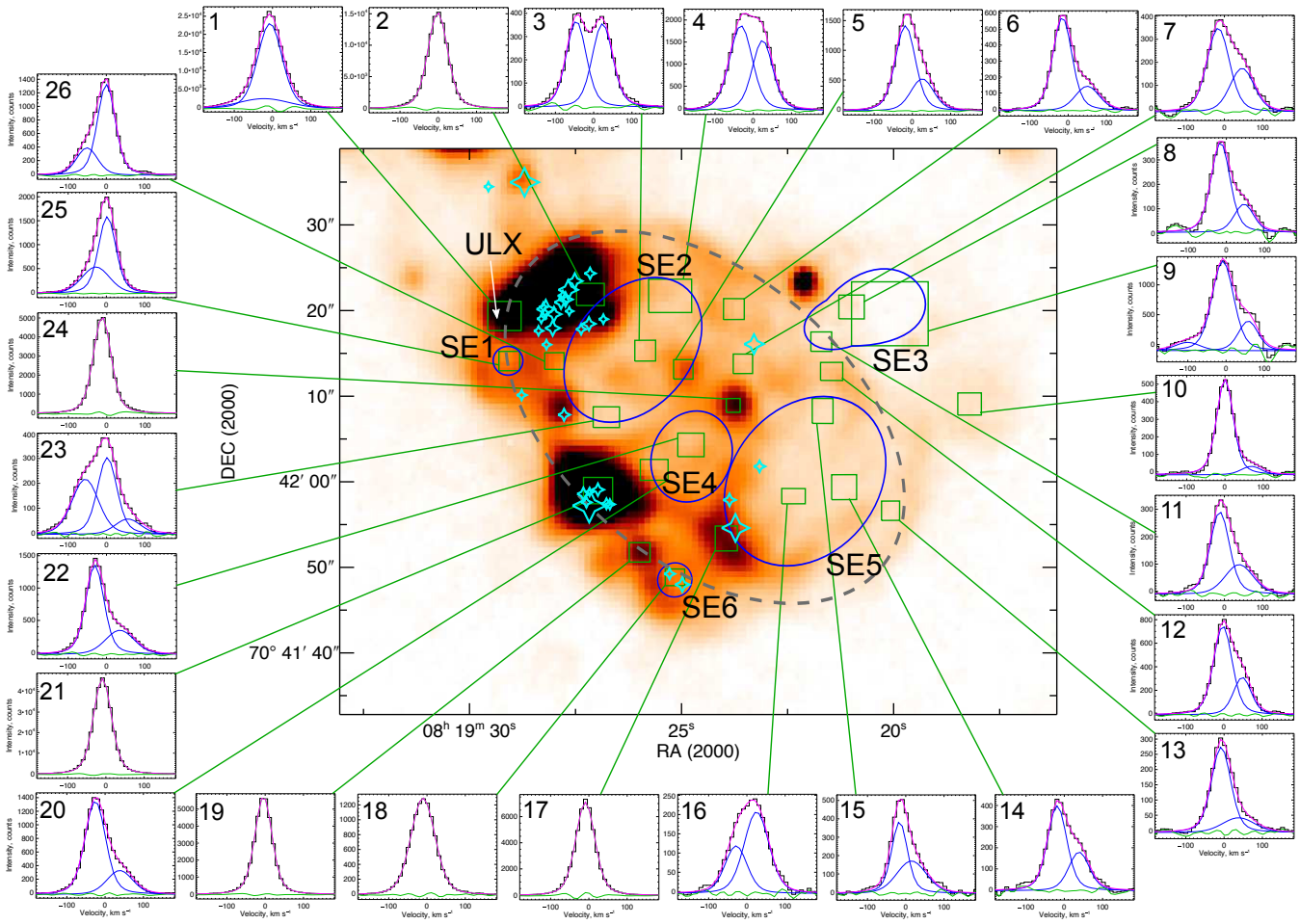

Figure 7. Hα image of the SE complex; Hα line profile examples obtained by integration inside the green borders in the image. The results of 1, 2 or 3 component Voigt fitting are shown: blue colour denotes the individual components, while the fitting model is shown in magenta colour. Green colour is used to show the residuals after subtraction of the model from the observed line profile. Blue ellipses in the image mark the positions of faint shell-like structures identified in the area. A grey dashed ellipse shows the location of the neutral-gas shell identified as a result of the analysis of the H I PV diagrams and associated with the observed multishell complex of ionized gas. Light blue asterisks denote the location of OB-stars identified by the analysis of *HST* colour–magnitude diagrams; their sizes are proportional to their luminosity.

complex. The location of this H I shell coincides with that of the H I cavity #27 identified by Weisz et al. (2009a).

While the bright H II regions are located in the direction of dense parts of the H I SGS, the central part of the SE complex resides in a more exhausted medium (see the top panel of Fig. 5). Such density distribution allowed one to expect the highest expansion velocities of ionized gas in the centre of the complex. We found 3 faint expanding ionized superbubbles there which possibly interact with each other and 3 superbubbles located at the periphery of the complex (including two young compact supershells SE1 and SE6).

As is evident from the Hα line profiles decomposition (see Fig. 7), the ionized gas kinematics is inhomogeneous in the whole SE complex. This area exhibits the most clear signs of the expansion of shell-like structures of ionized gas. For example, the northern SE2 superbubble reveals clear two-component Hα line profile in its centre corresponding to the expansion velocity of about 37 km s^{-1} – one of the highest among the ionized superbubbles we found in Ho II. The 'velocity ellipse' for SE2 – another evidence of its expansion – is also clearly seen in the PV diagram constructed in the direction of its elongation (#5 in Fig. 4).

The bright HSK 70 region containing the ULX source Holmberg II X-1 and a young star cluster is located in the north-eastern part of one of the inner shells. We will analyse the kinematics of ionizing gas in its neighbourhood in our forthcoming paper (Egorov et al. 2016). The young cluster in that nebulae is the main source of ionizing photons in the complex. Another sources of the ionizing radiation are the star cluster in HSK 67 nebula (in particular, the brightest one among the selected O stars) at the south-east of the complex and 10 OB stars spread inside the complex. As it follows from Table 4, the amount of ionizing photons emitted by the observed OB stars is consistent to that needed to ionize gas in the complex.

Note that massive OB stars are absent inside all the mentioned ionized superbubbles (except the compact one SE6) or located at their rim close to the bright nebulae. It

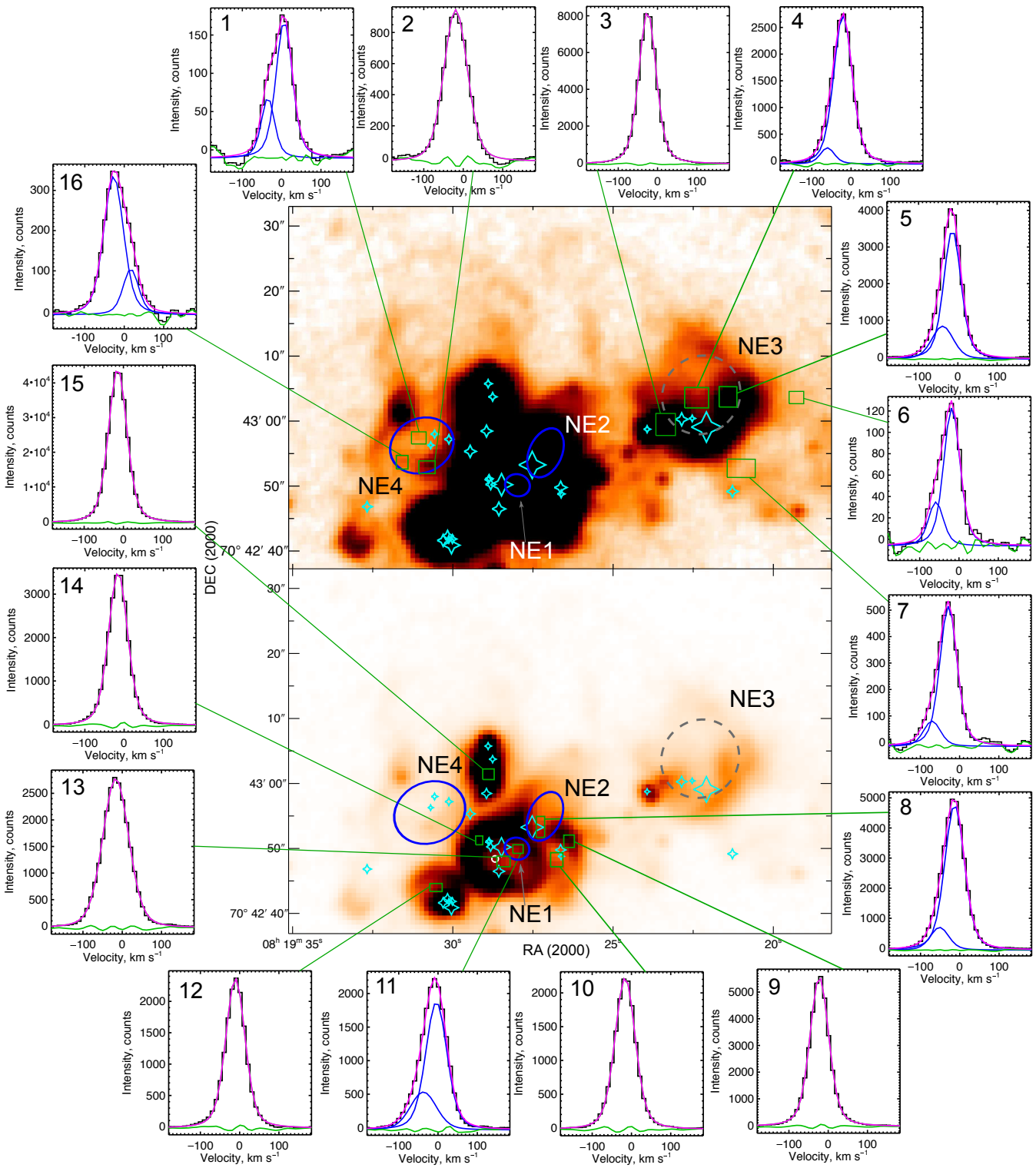

Figure 8. The same as in Fig. 7, but for the NE complex. The top and bottom images correspond to the same area with different contrast. White circle shows the area of He II 4686 Å emission detected in Egorov et al. (2013).

may indicate that the source of mechanical energy needed to support the expansion of these structures can stem from leakage of wind mechanical energy from the bright H II regions through their broken irregular shells. An order of magnitude supports such an assumption: the two OB stars inside the SE6 shell can give the wind energy leakage of $\dot{E}_w \sim 10^{37}\eta$ erg s^{-1} ($\eta < 1$ is the leakage efficiency), where the values $\dot{M}_w = 10^{-5}$ $M_\odot$ yr^{-1} and $v_w = 2000$ km s^{-1} corresponding to the high end range Markova & Puls (2008) have been accepted for the mass-loss rate and wind velocity.

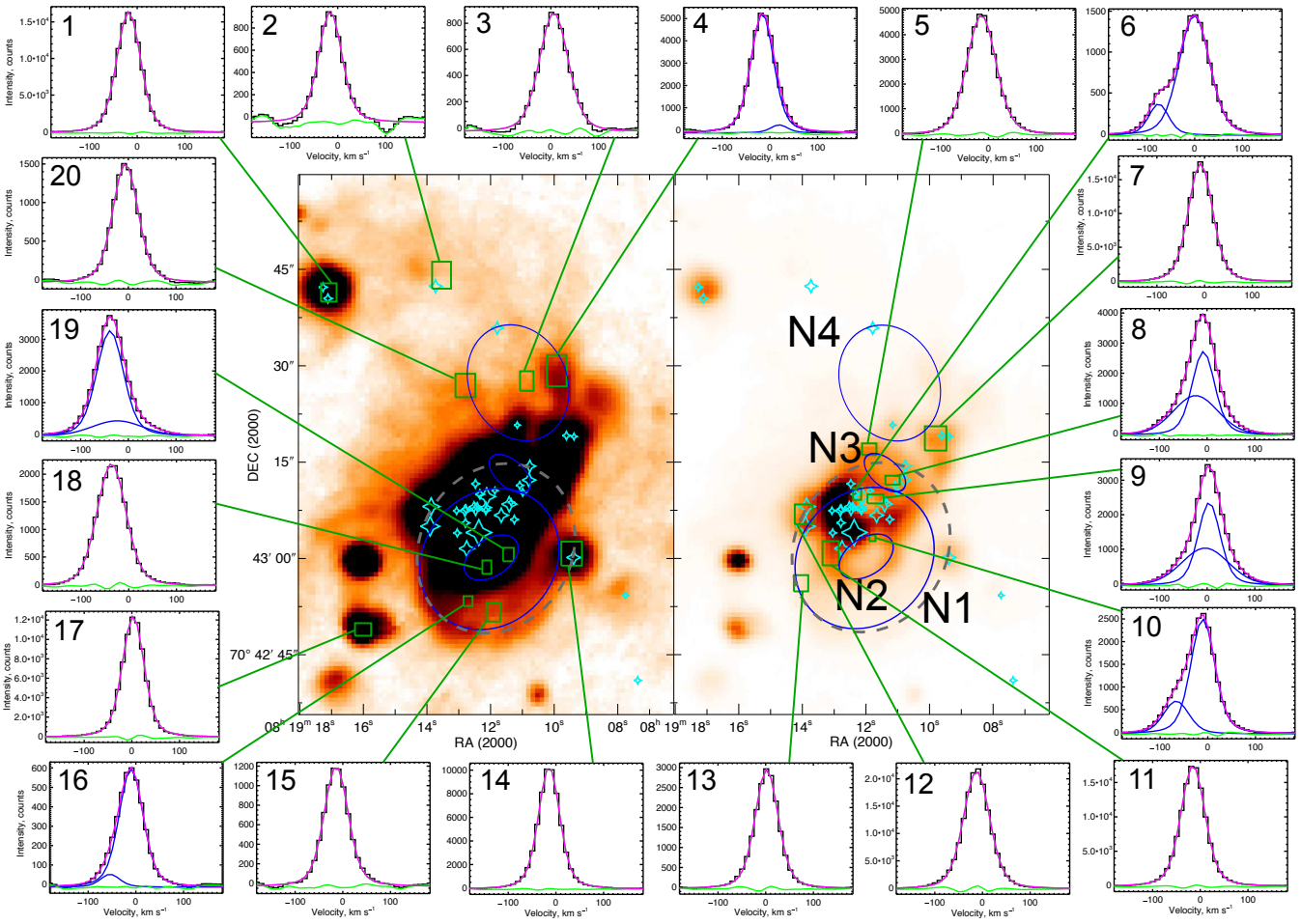

Figure 9. The same as in Fig. 7 but for the N complex. Right and left images correspond to the same area with different contrast.

On the other hand, the total radiation energy loss in the shell can be readily estimated as $\dot{E}_r \sim 3\times10^{36}$ erg s^{-1}, while the kinetic energy consumption $\dot{E}_k = \dot{M}_{\rm sh}V_{exp}^2/2 \sim 10^{36}$ erg s^{-1} with $\dot{M}_{\rm sh} = 4\pi\rho R^2 V_{exp}$; here we accepted the parameters for the expanding shell SE6 as shown in Table 3, and gas density is assumed $n \sim 0.3$ cm^{-3} (see estimates below); for the cooling rate, we assumed the typical value $\Lambda/(n_{\rm H}n_e) \simeq 2\times10^{-24}$ erg cm^3 s^{-1} at $T_e \simeq 8000$ K (Draine 2011). It is seen that $\eta \simeq 0.4$ would be sufficient to replenish energy consumption in this shell.

As we pointed out above, the presence of the faint extended structures jointing the H II regions and of the H I supershell around the whole SE star-forming complex confirms that we are dealing with a single entity here.

NE complex (HSK 71, 73, 74, 56 and 59)

The filaments of ionized gas between HSK 56, 59 and 73 H II regions as well as the brighter emission between HSK 71, 73 and 74 are clearly seen in our deep Hα image (Fig. 8). It allows us to consider these structures as a single star formation complex.

The observed Hα profiles in this area are mostly single, albeit 4 faint compact expanding shell-like structures of ionized gas can be identified (see Fig. 8). Except them, several faint shell-like structures without any signs of expansion are observed it the north part of the complex. Broadening of the Hα profile is observed inside the ring-like H II region HSK 73, in whose centre we have earlier found (Egorov et al. 2013) an object with a rather broad He II 4686 line (the area with the observed He II emission is shown with a white circle in Fig. 8). This nebula does not reveal a clear evidence of expansion; we found signs of its expansion only at the north-western part of the region, where the young compact shell NE1 is located. The more extended shell NE2 we found at the periphery of HSK 73 region.

The complex NE is located in a dense H I cloud on the outer side of the SGS rim. Its northern part penetrates into the adjacent H I supershell (see Fig. 1). Such distribution of the neutral gas density in the complex is consistent with the observed faint arcs of ionized gas extended to the north of bright H II regions over more than 350 pc (see Fig. 8). The faint supershell NE3 between HSK 56 and 59 nebulae is also north elongated.

In the same way as in the SE complex, the absence of massive stars in the centre of all superbubbles in the NE complex (excluding NE4) indicates the necessity of mechanical energy to escape from the bright H II regions in order to drive it.

Massive OB stars – the sources of required ionizing Ly-

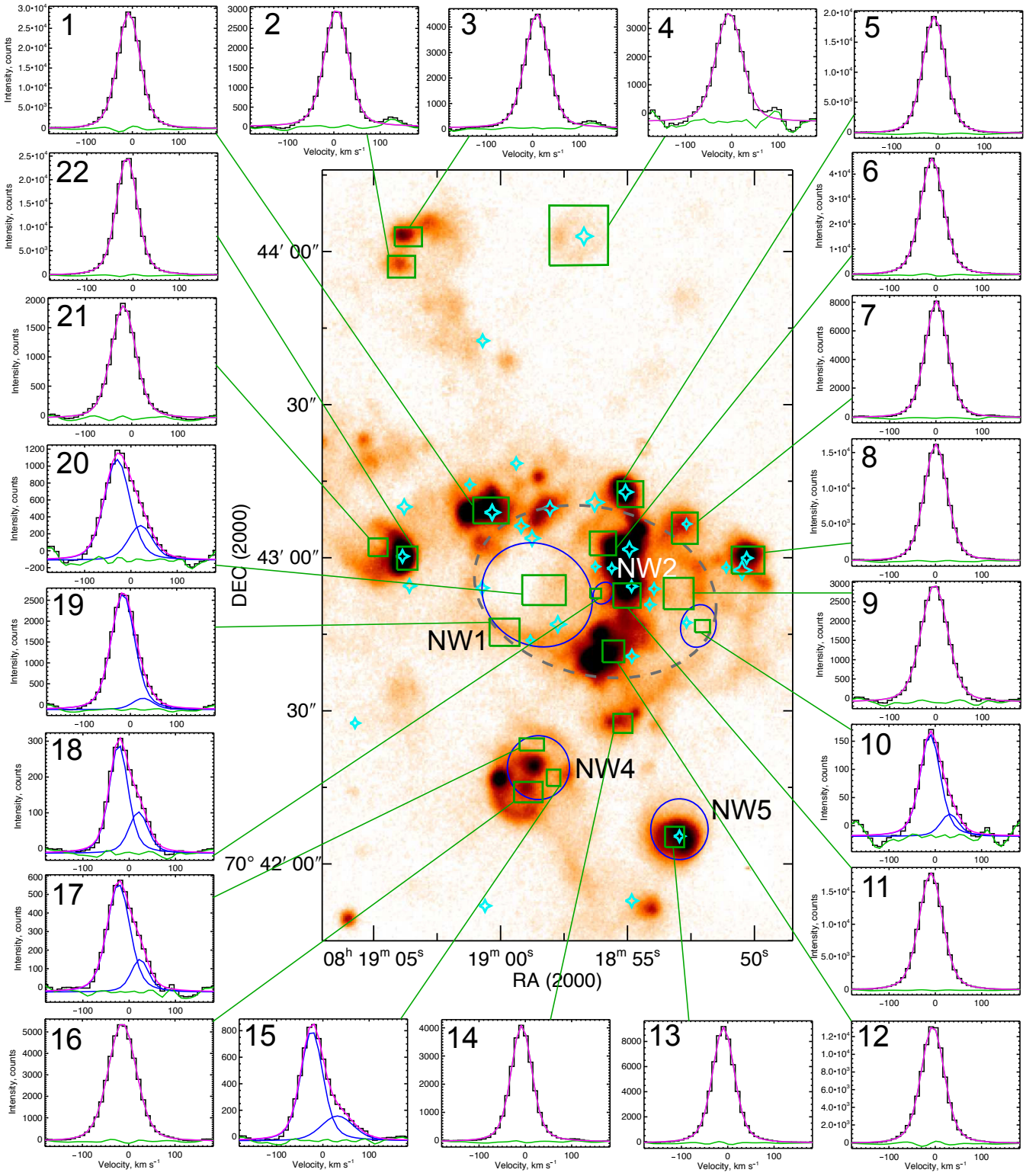

Figure 10. The same as in Fig. 7 but for the NW complex.

man continuum photons, are spread in the whole NE complex and do not reveal concentration to the star clusters as it was for the SE complex. The only poor star cluster is located at the south-eastern part of the complex. As it evident from Table 4, the number of identified OB stars is enough to ionize the gas in the complex.

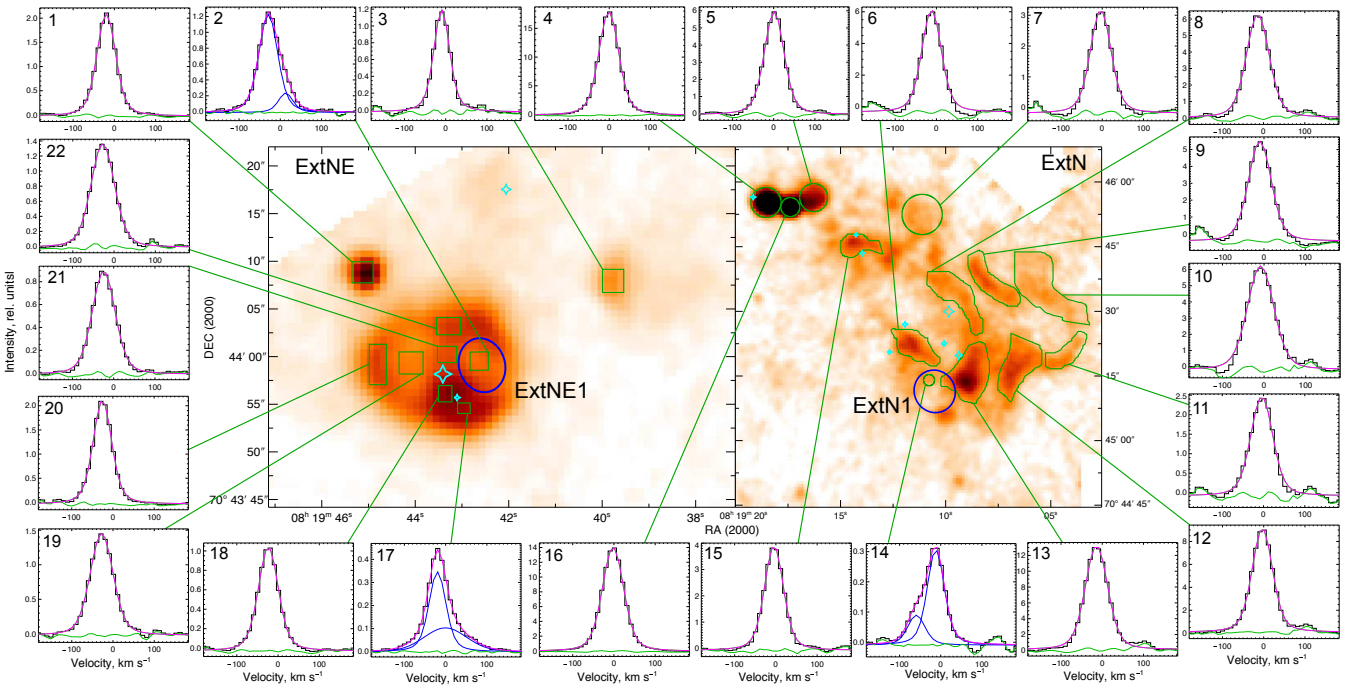

Figure 11. The same as in Fig. 7 but for the ExtN (right) and ExtNE (left) complexes.

N complex (HSK 45 and 41)

We refer to the brightest H II region in the galaxy, HSK 45, (and also adjacent compact nebula HSK 41) as an individual complex. Its Hα images and kinematics reveal a number of interacting shell-like structures inside these H II regions, see Fig. 9. The expansion velocity of the H II region HSK 45 may be as high as 35 km s^{-1}, albeit the observed kinematic perturbations are most likely due to the interaction between 3 identified local shells. Based on the ionized gas kinematic analysis, we found the N2 shell to be located inside the older and more extended superbubble N1. For example, the evidence of such a structure is a more deep 'dip' at the velocity ellipse in the PV diagram constructed through the both shells (see position 23 arcsec along PV diagram #3 in Fig. 4).

The complex is located at the site of probable collision of three H I supershells – the SGS and two other to the north of it. The H I kinematics reveals the existence of expanding H I shell (previously unknown) that covers the whole complex. Signs of its expansion are clearly seen on PV diagram #1 (HI) at positions of 100 − 130 arcsec along the slice in Fig. 4.

Massive OB stars mostly located in the centre of the HSK 45 nebula are the sources of energy for ionization and maintaining the expansion of the observed emission structures. Our deep Hα and [S II] images of the region reveal extended arcs of ionized gas in the northern part of the complex. These structures show enhanced ratios of I([S II])/I(Hα), although their position on the diagnostic diagram I([O III]5007)/I(Hβ) vs I([S II])/I(Hα) does not indicate the clear signs of collisional ionization by shocks (see Section 6.4 for details). The relatively old faint shell N4 shows up among these structures. Evidence of its expansion follows from PV diagram #4 in Fig. 4. Most likely, the mechanical energy leakage from HSK 45 region should be a source of the necessary energy to drive its expansion.

Decomposition of the Hα profile reveals the presence of a broad component inside the bright region HSK 45 (see profiles # 8, 9 and 19 in Fig. 9). This component might be caused by the influence of the shock waves from some energetic source, e.g. the Wolf–Rayet star, to the ISM. This idea is supported by findings of Hong et al (2013) who identified signs of shocks in several areas in the central part of the HSK 45 nebula from the *HST* observations.

NW complex (HSK 15, 16, 17, 20, 25, 26)

This is a chain of relatively compact bright H II regions in the northern part of the complex of ongoing star formation in the SGS surrounded by faint shell-like structures of ionized gas with the signs of its expansion (see Fig. 10). The bright H II regions exhibit a single-component Hα profile which is broadened in some places. Their possible expansion velocities do not exceed 11 km s^{-1}.

The complex NW located in the direction of the dense part of the H I SGS rim, albeit the neutral hydrogen density varies considerably there. As it follows from the bottom panel of Fig. 5, the location of the bright nebulae basically correlates with the H I column density. Kinematics of the neutral gas reveals the existence of an H I shell that covers the central part of the complex. The chain of the bright H II regions is located in the central part of that H I shell.

According to Weisz et al. (2009a), the peak of star formation was in the direction of the NW complex about 20 Myr ago. Indeed, the GALEX images reveal bright FUV emission there (see Fig. 1) which poorly correlates with the distribution of the Hα emission. As the FUV emission indi-

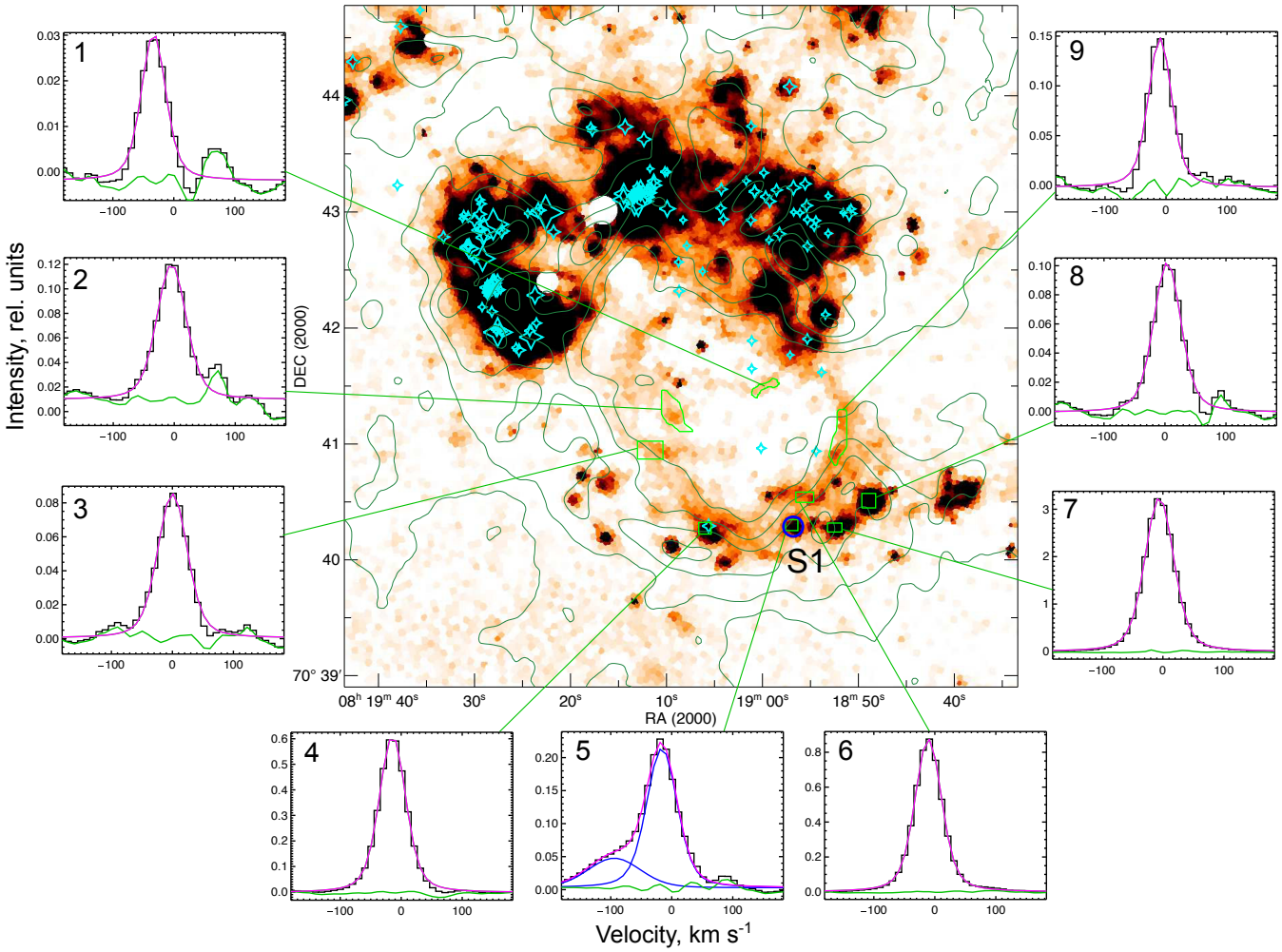

Figure 12. The same as in Fig. 7 but for the whole region of ongoing star formation in the walls of the SGS. The Hα image shown here was obtained by applying of adaptive binning with the signal-to-noise ratio equal to 30. Green contours show the lines of equal H I column density.

cates a recent star formation, while Hα emission corresponds to the ongoing star formation, such disagreement in their distribution might be an evidence for the triggering of the ongoing star formation by the feedback of the recent star formation episode in the chain of compact H II regions of the complex.

The distribution of massive OB stars does not show any concentration to star clusters. The expansion of only 2 of 5 ionized superbubbles could be explained by the stellar wind of OB stars located inside them. The mechanical energy leakage from the adjoint bright H II regions can provide the necessary energy to drive the expansion of another 3 superbubbles. As it follows from Table 4, the amount of Lyman continuum photons from the identified OB stars is enough to ionize the gas in the NW complex.

External complexes (ExtN and ExtNE)

Let us analyse now the two regions marked as ExtN and ExtNE in Fig. 2 which are not connected with the walls of the SGS discussed in this paper. As is evident from Fig. 1, both these regions are located in the rims of H I supergiant shells located next to the SGS. Note that the ExtNE region is relatively compact and bright when observed in the Hα line and surrounds the compact central source of UV radiation. Here the presence of the broad component of the Hα profile in the brightest part of the complex is immediately apparent, as well as the expanding shell ExtNE1 east of it (Fig 11). Unfortunately, we cannot determine the boundaries of this shell and, hence, its age with certainty.

The ExtN region, in turn, appears as a complex of filamentary diffuse structures surrounding compact UV sources. It is fair to assume that Hα radiation is caused by younger regions in the area, where star formation is triggered by the previous generation of stars located in accordance with the FUV emission. We found the only ionized superbubble having signs of its expansion (ExtN1) in the southern part of the complex. Generally, the Hα profile in both northern regions can be well fitted by a single unbroadened component implying that the expansion velocity of ExtN and ExtNE does not exceed 11 km s^{-1}.

Despite the scarcity of massive OB stars inside both

complexes, their energy input is enough to ionize the gas there. The low brightness of these H II complexes is consistent with a small number of sources of ionizing radiation. Note that due to the above-mentioned lack of information about stellar population of the north-western part of the complex, in Fig. 11 and in Table 4, we indicate only a part of OB stars which probably influence the complex.

Internal ionized supershell in SGS.

Our deep Hα images allowed us to identify a faint diffuse component of ionized gas inside the SGS close to its walls which is not seen in the *HST*/ACS and any previous images of the galaxy. We observed an Hα line emission inside this SGS with an average brightness level of $3-6\times10^{-18}$ erg s^{-1} cm^{-2} arcsec^{-2} and [S II] line emission with an average brightness level of about $0.5-1\times10^{-18}$ erg s^{-1} cm^{-2} arcsec^{-2}. The Hα profile in the inner ionized supershell is narrow and symmetric. Based on the difference of the line-of-sight velocities in different parts of this supershell, we may conclude that its expansion velocity does not exceed $10-15$ km s^{-1} which corresponds to the expansion velocity of the neutral SGS.

Several filaments of ionized gas are observed in the central part of the area covered by internal ionized supershells. Probably, they correspond to the emission projected toward the supershell region. Hα line profile #1 which shows the line-of-sight velocity shifted at almost 30 km s^{-1} from the mean velocity of the supershell, supports this idea.

We denote the area that corresponds to this faint supershell as Int.shell in Table 4 and Fig. 2. Several compact H II regions projected to the Int.shell, are located in the southern part of the H I SGS. One of them (the S1 shell in Table 3 and Fig. 12) shows the clear evidence of expansion.

6 DISCUSSION

6.1 What triggered star formation in Ho II?

Detailed multicolour *HST* photometry of the stellar population inside each supergiant H I shell in the Ho II galaxy reported by Weisz et al. (2009a) (see also references therein) revealed stars of several age groups rather than single coeval clusters as previously believed. It stimulated a new currently widely accepted model: neutral supergiant shells were formed from several generations of stars over several hundreds million years.

The main criterion of current starburst – the Hα emission in the neighbourhood of a newly formed cluster of young stars – appears for $1-2$ Myr and rapidly fades (in about 10 Myr – the main-sequence lifetime of OB stars and the time-scale of coherent existence of young star clusters Lada & Lada 2003). The UV radiation of massive young stars of the cluster reaches its maximum at about 5 Myr, and FUV decays over much longer time-scale limiting the time period, when the traces of star formation remain visible to $\simeq 100-150$ Myr (O'Connell 1997; Stewart et al. 2000). That is why in terms of accepted model of supergiant shells formation, the Hα emission and 24 μm IR radiation which trace the sites of current SF in Irr galaxies and, in particular, in Ho II, do not always correlate with the location of giant H I supershells of at least several hundred Myr old.

Two questions concerning star formation processed in Irr galaxies remain to be of interest today: what actually triggers the ongoing star formation in a particular region of a galaxy? And how does the structure and kinematics of giant H I cavities and shells change under the influence of new episodes of star formation in their walls? The analysis of the structure and kinematics of H II regions in the walls of the SGS in the Ho II galaxy that we perform in this study is an attempt to shed certain light on the problem. In this section, we discuss the probable mechanism responsible for initiation of the ongoing star formation in Holmberg II.

An analysis of deep $H\alpha$ images of 51 Irr and diffuse galaxies allowed Hunter et al. (1993) to discover a distinguishing feature of Ho II, which consisted of the very local disposition of H II regions. The authors formulated the question: why there are so few shell-like ionized structures despite the presence of many neutral supergiant shells which most likely have been produced by the stellar wind and SN explosions of rich OB associations? As we pointed out above, all local star-forming complexes — the brightest emission nebulae as well as the brightest UV and IR regions — are located in the northern wall of the most extended H I cavity in the galaxy (see Fig. 1). Such localization makes the question about the nature of ongoing star formation in Ho II to be more intriguing – why H II regions are observed mostly in the north part of SGS, but not spread over it?

One of possible explanation of such star formation distribution might be its occurring in the densest gaseous clouds in the galaxy. Does the locations of star-forming regions in Ho II correlate with the gas volume density in the SGS? To answer to this question, we estimated the H I volume density from the LITTLE THINGS data. We constructed the 21-cm line intensity map using the technique described by Walter et al. (2008) based on the H I 21 cm line intensity distribution. To convert column density into volume density, we assumed that the scale height of the H I disc and its inclination to be $h = 400$ pc (Banerjee et al. 2011) and $i = 47^\circ$ (Oh et al. 2011) respectively.

As a result, we establish that the distribution of H I volume density in the SGS discussed, where regions of ongoing star formation are located, is, on the whole, uniform with $n_{\rm HI}$ varying from 0.3 to 0.7 cm^{-3}. The inferred densities agree with the previous estimates of the density in the SGS: 0.5 cm^{-3} and 0.3 cm^{-3} according to Bagetakos et al. (2011) and Puche et al. (1992) respectively.

The 'central arc' of bright ionized nebulae in the Ho II galaxy is indeed located in the region of the highest HI column density. However, the average column density of neutral gas at this location does not substantially exceed the density in the southern wall of the SGS which contains small separate star-forming regions but with no extended Hα emission complexes similar to the regions in the 'central arc' (see Fig. 1).

Moreover, star formation in galaxies may occur in environments with sufficiently low densities. Recent studies fail to reveal the so-called gas surface density threshold above which star formation begins; at lower densities, the star-formation efficiency decreases more rapidly with the decrease of gas density but does not vanish even at $\Sigma_{\rm HI+H_2} < 0.5$ M$_\odot$ pc^{-2} (see Bigiel et al. 2008, 2010; Zasov & Abramova

2012; Abramova & Zasov 2012 and references therein) and, apparently even at lower densities (Shi et al. 2014). Summing up, we can't explain the observed location of H II regions in Ho II by the gas density distribution.

Our study shows that the region that separates the SGS discussed and the giant irregularly shaped northern cavity consisting of several shells adjoining each other in the sky plane is characterized by a very non-uniform structure and the greatest local variations of the neutral-gas velocity in the galaxy. The distribution of H I velocity dispersion along the SGS discussed here shows insignificant variations – approximately from 7 to 16 km s^{-1}. However, it is interesting to verify whether these variations are related to ongoing star formation in the SGS rims. In order to answer this question we compared pixel-by-pixel the H I velocity dispersion and Hα flux that traces star formation rate.

The procedure had several steps. First of all, we performed a Gaussian convolution of our Hα image in order to obtain the same spatial resolution as for the H I LITTLE THINGS data. We then resized the convolved Hα image in order to obtain the same pixel scale with an H I velocity dispersion map. After that, the pixels corresponding to the bright H I rim of the SGS were selected for a further analysis. We constructed a 2D histogram of the Hα flux and H I velocity dispersion distributions among these pixels. The resulting histogram is shown in the top panel of Fig. 13. We also show the mean H I velocity dispersion and its standard deviation for each flux bin.

As is evident from the constructed histogram, the H I velocity dispersion in the SGS does not change in the areas with a very low Hα flux. However, starting from $F(\mathrm{H}\alpha) \simeq 2 \times 10^{-18}$erg s^{-1} cm^{-2} arcsec^{-2}, velocity dispersion begins to show an increasing trend.

The observed dependence can be explained by two factors. First, the H I velocity dispersion may have become higher because of the collision of the SGS with the above northern supershells resulting in ignition of star formation in this region. Second, the ongoing star formation itself may have an effect on the SGS by increasing the H I turbulence level near bright H II regions. In the bottom panel of Fig. 13, we show the similar histogram for another supergiant shell we previously studied (Egorov et al. 2014) located in IC 2574 galaxy. In contrast to Ho II SGS, the morphology of a supergiant shell in IC 2574 does not reveal any signs of its interaction with neighbouring shells, and we do not see any clear correlation between the H I velocity dispersion and the Hα flux for that case. This allows us to prefer the first explanation of the dependence observed for the Ho II galaxy.

The above facts and considerations suggest that the last episode of star formation in the Ho II galaxy, which we observed as areas of bright H II regions and shells, was triggered by the collision of two above mentioned giant H I shell-like structures (or, possibly, by the collision of multiple shells that produced them).

The mechanism of star formation triggered by the collision of supergiant shells is well known (see Chernin et al. 1995); many colliding supergiant shells with star formation have been found in the LMC (see the references in the above paper).

One of the most striking examples of this process is clearly observed in the irregular Local group galaxy IC 1613, where the region of ongoing star formation is localized at

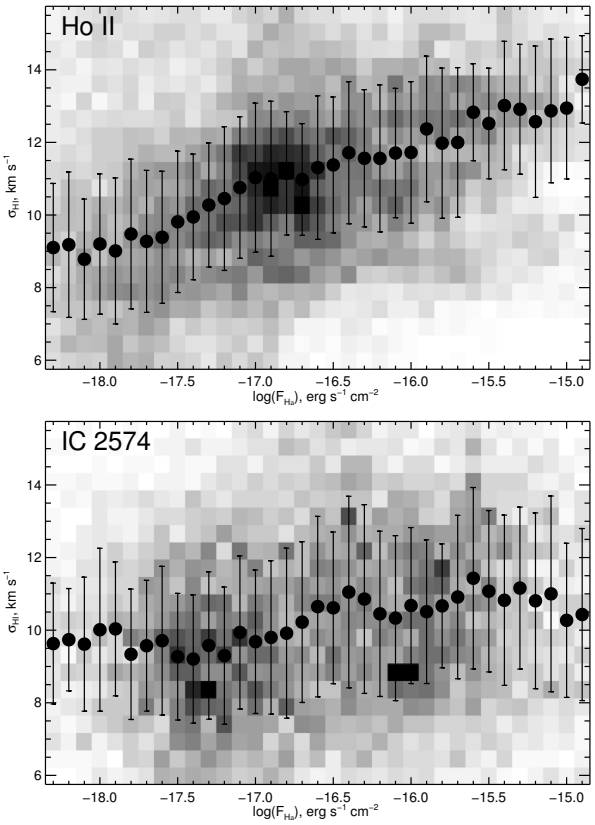

Figure 13. 2D histogram of the Hα flux and H I velocity dispersion along the SGS in Ho II (top) and IC 2574 (bottom) galaxies. Black points and bars denote the mean value and standard deviation of the H I velocity dispersion for each Hα flux bin.

the periphery of a supergiant H I shell at the place of its collision with another supergiant shell located north of it (see Lozinskaya 2002).

Another example of this type can be found in the NGC 6946 galaxy: a complex of H II regions, which is the second largest such complex in the galaxy, is located at the interface between two neutral gas cavities #107 and #106 identified by Boomsma et al. (2008), see also Efremov, Afanasiev & Egorov (2011).

Note that the collision of supergiant shells by itself is, generally speaking, also a natural consequence of the interaction between the collective wind and supernovae and the ambient gas over a more extended scale length and timescale.

6.2 Complexes of current star formation

Faint extended filamentary structures of ionized gas identified in this study, which connect individual bright H II regions, have changed our understanding of the regions of triggered star formation in the galaxy. It is evident that current sites of star formation are not 'chains' of bright nebulae in the walls of the HI SGS, as previously thought, but rather unified extended star-forming complexes with sizes extending up to several hundreds pc, i.e. comparable to the size of the SGS. The conclusion that the structures considered are single entities is further corroborated by our discovery

of faint neutral shells surrounding the complexes SE, N and NW.

The formation of such unified complexes can be understood in terms of the current view on the feedback between stars and the ambient gas given the strong inhomogeneity of gas in the SGS walls. The UV radiation of massive stars ionizes the surrounding gas and creates bright H II regions. At the outer boundary of a dense parent cloud, the ionization front penetrates further into the tenuous medium creating 'blisters' on the side of the dense cloud (a so-called 'champagne effect') according to the model by Tenorio-Tagle (1979). Radiation and stellar winds form faint shell-like structures in the tenuous ambient medium. These structures resemble faint filamentary structures observed in the SE, NE, N and NW complexes. As expected in terms of this model, the observed expansion velocity of faint shell-like formations exceeds the expansion velocities of the bright and more compact nebulae (see Section 4). Note that the age of faint extended structures should be close to that of bright and more compact structures if these are unified sites of star formation.

Unfortunately, the accuracy of age determination for individual objects in these unified complexes of star formation listed in Table 3 leaves a lot to be desired because of too many uncertain factors involved.

We discussed the errors of age estimations based on the equivalent width of the H-beta line in our earlier paper Wiebe et al. (2014). The main ones are the assumption about a single starburst in a given H II complex and the internal extinction (see also Stasińska & Leitherer 1996).

The age determined by Stewart et al. (2000) should be treated as the mean age of stars in the aperture because of the fact that a single-generation model is used to interpret a flux from what is potentially a mix of populations of slightly different ages. To compensate for this uncertainty, regions are classified into four age groups. According to the authors, when comparing regions the actual age cutoffs for each group should be ignored and groups should be just thought to consist of relatively very young, young, intermediate-age or older star-forming regions.

In principle, the most accurate age estimate is the kinematic age if the expansion velocity and the radius of a shell are correctly determined. However, in the case of Ho II the spatial resolution is insufficient to construct the 'velocity ellipse' in each nebula. We attempted to estimate the expansion velocity from the split of the position-velocity diagrams, however, no such evidence was revealed for bright regions. For this reason, we have estimated the expansion velocities of the nebulae from individual profiles, i.e. without any guarantee that they refer to the region of the most high-velocity motions. Furthermore, the irregular structure of the H II regions complicates a correct determination of the shell radius.

Given these uncertainties, the ages estimated by different methods (listed in Table 3) are consistent with our conclusion about single complexes of current star formation in the galaxy, which combine several bright nebulae and the associated weak shell-like structures.

In Section 5, we report the estimations of the amount of ionizing radiation from the young massive stars located inside the complexes. It follows from Table 4 that it is sufficient to account for the observed Hα flux for all the complexes.

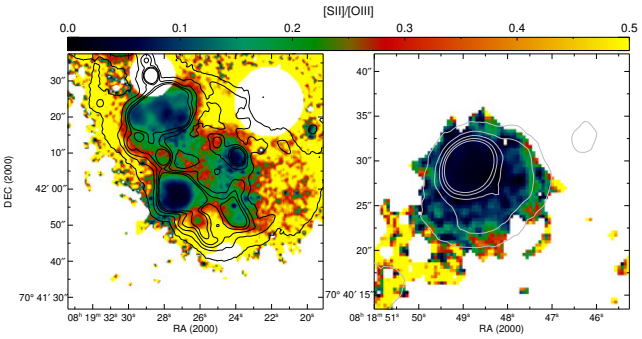

Figure 14. [S II] 6717,6731Å to [O III] 5007 emission-line ratio maps for the SE complex (left) and the H II region at the south-west of the SGS rim (right). Isophotes correspond to the Hα flux levels $(5, 15, 25, 35 and 45) \times 10^{-17}$ erg s^{-1} cm^{-2} arcsec^{-2}. The regions contaminated by the foreground stars are masked.

In faint external complexes the energy of stars is more than sufficient for ionizing the gas. The 'extra' photons from these complexes probably leak from these low-density and high-humidity complexes.

Pellegrini et al. (2011) proposed the method of distinguishing between density- and radiation bounded H II regions based on the I([S II])/I([O III]) ratio map. The main idea of the method is that for an optically thick nebula one should observe the increased I([S II])/I([O III]) ratio at the edges of a region, while in the optically thin case the low ionization zone with the enhanced [S II] emission might not appear. We have applied this method to the galaxy Holmberg II and found that almost all regions of ionized gas show the ionization structure that is typical of optically thick H II regions – they exhibit the outer shell of the enhanced I([S II])/I([O III]) ratio surrounding the [O III] dominated core corresponding to the hot regions near the ionization sources. As an example of such structures, we show the I([S II])/I([O III]) map for the SE complex on the left panel of Fig. 14. Note, however, the increased contribution of [O III] emission outside the border of the northern H II region probably caused by the ionizing radiation leakage toward the centre of the SE complex. The only optically thin region in the galaxy that does not represent such a [S II] shell is the compact H II region at the south-western part of the SGS (shown in the right panel of Fig. 14). Thus, we may expect large escape fraction of ionizing radiation from this region, but also we cannot rule out the possible leakage from other H II regions due to their porosity. Strictly speaking, this method allows us to identify density-bounded regions, but the regions which look like radiation-bounded in the I([S II])/I([O III]) maps still might be optically thin.

6.3 Internal ionized supershell in SGS.

We were the first to identify a faint diffuse internal supershell of ionized gas inside the SGS which was not seen in the *HST*/ACS images. The expansion velocity of the inner shell coincides with the expansion velocity of the neutral SGS.

The I([O III]5007)/I(Hβ) vs I([S II])/I(Hα) diagnostic diagram shown in Fig. 15 suggests that the increased values of these ratios corresponding to a gas glow behind the shock front is practically not observed in the galaxy including the

region inside the the SGS. It can be concluded from this that the nature of the ionized gas emission inside the SGS in the Ho II galaxy differs from that we have discovered inside the supergiant H I shell of the IC 2574 galaxy. Based on the observed increased I([S II])/I(Hα) and I([N II])/I(Hα) line ratios of diffuse gas in the IC 2574 SGS, we concluded (Egorov et al. 2014) that it should be similar to those of the extra-planar diffuse ionized medium (DIG) in spiral and irregular galaxies. Owing to that similarly to the DIG, we explained the faint diffuse ionized gas emission inside the SGS in IC 2574 as a result of leakage of both the ionizing photons and mechanical energy from the bright H II regions. In the case of Ho II, the location of the regions corresponding to the ionized internal superbubble on the diagnostic diagram (Fig. 15) is indicative of the photionization mechanism of gas emission there.

The analysis of the FUV morphology of the galaxy presented by Stewart et al. (2000) shows the large region of faint diffuse FUV emission extending to the south-west of the central arc of bright H II complexes. This structure is clearly seen in Fig. 1. The relatively bright regions of FUV emission, denoted as star-forming regions 23, 35, 36 and 37 in the list of Stewart et al. (2000) and selected by the above authors as areas with FUV and no Hα emission and also fainter regions practically completely fill the inner supergiant shell (see Fig. 1). However, the observed FUV emission comes from the regions, where intensive star formation occurred 20–60 Myr ago (Weisz et al. 2009a) and hence there was a lack of ionizing Lyman quanta. What is responsible for the creation of this internal ionized supershell in SGS then?

As it follows from Fig. 12, five identified OB stars are located inside the internal Hα superbubble near its north-western edge. Their photometry shows that all of them are massive O stars. Correspondingly, these stars are most likely the main source of ionizing photons. Thus, according to Table 4, the amount of ionizing quanta from these stars is consistent with the value necessary to maintain the observed Hα flux. Note that the pure diffuse component of the ionized superbubble is denoted as 'Int.shell (diff)' in Table 4, while 'Int.shell (all)' means the whole region including the compact bright H II nebulae at the rim of the superbubble. Additional sources of ionizing radiation could be located in the south-western chain of bright compact H II regions, for which there are no available data about their stellar population.

However, a certain contribution of energy leakage to the ionization of the superbubble can not be ruled out. The latter is supported with the fact that the brightest nebula at the southern rim of the superbubble seems to be optically thin (see Fig. 14 and Section 6.2) that might cause the high fraction of ionizing photons escape.

Summing up, the ionized internal supershell was created most probably by the influence of ionizing radiation of 5 O stars located at its interior and of the additional energy leakage from nearby bright H II complexes to the internal walls of the H I SGS.

In addition, a continuing mechanical energy input from stellar activity, winds and SNe explosions, may also act on to the internal side of the SGS and contribute to its dynamics. For instance, speaking about the SE complex shown in Fig. 7, it can be clearly seen from rough estimates that the total mechanical energy input from the stars inside the shell $\dot{E}_{\rm wind} \sim 10^{38}$ erg s^{-1} and the shell kinetic energy consumptions $\dot{E}_k \sim \sum 4\pi\rho R^2 v_s^3 \sim 2\times10^{38}$ erg s^{-1} are marginally equal (the gas density $n \sim 0.3$ cm^{-3} is assumed, see above).

Shock waves from a stellar wind and SNe evacuate most of gas into the shell, so that the cavity remains filled mostly by wind and SNe ejecta with a very low density. For instance, when a supergiant shell is produced by multiple SNe explosions the remaining density might be as low as $\lesssim 10^{-4}$ of the ambient density (Sharma et al. 2014). Even if a much less violent energy release by ionizing radiation from underlying OB stars evacuates the gas, its density within the photo-ionized bubble remains as low as $\sim 10^{-2.5}$ (Henney et al. 2005; Henney 2007). One, therefore, estimates the gas density inside the bubble as $n_b \lesssim 5\times10^{-5}$ cm^{-3} if the bubble is due to SNe explosions, and as $n_b \sim 10^{-3}$ cm^{-3} otherwise.

In these conditions, the wind generated by massive stars inside the SGS acts from the interior and transfer momentum to the supershell. The free expansion phase of the wind continues until the swept-up mass equals to the wind-blown mass (see, e.g. Draine 2011)

$$t_0 \simeq 10^2 n_b^{-1/2} \dot{M}_6^{1/2} v_{\rm w,8}^{-3/2} \ {\rm yr}, \qquad (2)$$

where $\dot{M}_6$ in units $10^{-6} M_\odot$ yr^{-1}, $v_{\rm w,8}$ is the wind velocity in 10^3 km s^{-1}. This gives $t_0 \simeq 3\times10^4$ yr and the corresponding radius $R_0 \simeq 30$ pc for a SNe produced the SGS and an order of magnitude lower t_0 and R_0 for the case of a SGS driven by ionization fronts. Accounting that the massive stars inside the supershell (marked in Fig. 12) are located at larger distances – 100 to 400 pc, one can estimate pressure acting on to the shell as

$$P_{\rm w} = \rho_b \dot{R}_b^2 \simeq 10^{-8} \left(\frac{L_{36} n_b^2}{R_{1\ {\rm pc}}^2}\right)^{1/3} \ {\rm dyn\ cm^{-2}}, \qquad (3)$$

where L_{36} is the wind mechanical luminosity in units 10^{36} erg s^{-1}, R_b is the radius of a wind-driven shock in the ambient medium, $R_{1\ {\rm pc}}$ is its value in 1 pc. When the wind-driven shock acts on to the supershell it can support the expansion with the velocity

$$v_{\rm SGS} \simeq \left(\frac{P_{\rm w}}{\rho_0}\right)^{1/2} \simeq 0.8\times10^8 \left(\frac{L_{36}}{R_{1\ {\rm pc}}^2}\right)^{1/6} \frac{n_b^{1/3}}{n_0^{1/2}} \ {\rm cm\ s^{-1}}, \qquad (4)$$

so that for a SNe swept-up supershell with $n_b \sim 5\times10^{-5}$ cm^{-3} a star located at $R = 100$ pc (as, e.g. the brightest star in the left corner of the SE5 shell in Fig.7) would produce the velocity of the supershell of 6 km s^{-1}, while for $n_b = 10^{-3}$ cm^{-3} it would support $v_{\rm SGS} \simeq 13$ km s^{-1}. It is worth stressing that episodic wind and SNe explosions and the respective feedback during the whole evolution of the SGS can support gas density in the bubble at a level sufficient for transferring a proper momentum on its internal surface.

In those cases, when OB stars lie closer than R_0 to the SGS edge, they act on to the supershell by the expanding wind directly without transferring momentum through the gas inside the cavity. In this case, the shell velocity supported by wind would be a factor of $(L_{36} n_0 / R_{1\ {\rm pc}}^2 n_b^2)^{1/6}$ higher than the above estimate in Eq. (3). One may expect that the similar enhancement of the action of a stellar wind on the supershell would take place, when the wind propagates through low density tunnels inside the bubble.

Overall, one may think that energy release in the form of Ly-continuum photons and corpuscular winds emitted by massive stars inside the supershells does not only support their expansion, but also provides proper conditions for transferring momentum from stars to the walls and keeping them continuously expanding until star formation is exhausted.

6.4 Search for SNRs in the SGS.

Radio observations of the Ho II galaxy (Tongue & Westpfahl 1995; Braun et al. 2007; Heald, Braun & Edmonds 2009) revealed a continuum radio emission in the region of bright emission nebulae. The synchrotron component of radio emission was identified in the eastern chain of bright nebulae by Tongue & Westpfahl (1995) and this fact led the authors to suspect that these areas may contain supernova remnants. The detected polarized radio emission also coincides with this chain (Heald et al. 2009).

Hong et al (2013) identified the shock-ionized component via the line diagnostic diagram I([O III]5007)/I(Hβ) vs I([N II])/I(Hα) inside the HSK 45 nebula using the high resolution *HST* data.

Our spectroscopic observations (Egorov et al. 2013) did not allow us to identify the optical emission of these hypothetical supernova remnants and shock fronts by the I([S II])/I(Hα) line ratio.

We used our narrow-band images in the [O III] 5007Å, [S II] 6717,6731Å and Hα lines to construct the diagnostic diagram of I([O III]5007)/I(Hβ) vs I([S II])/I(Hα) ratios for each pixel of the galaxy. All the used line ratios were corrected by reddening using the mean value $E(B-V) = 0.05$ (Egorov et al. 2013). We calculated the values of Hβ fluxes from the Hα flux using the theoretical ratio I(Hα)/I(Hβ) for $T = 10000$ K (Osterbrock & Ferland 2006). The result is shown in Fig. 15. A black curve denotes the separation line between the regions with pure photoionization and composite (with a probably significant contribution of the shocks) excitation (Kewley et al. 2001). As follows from this diagram, almost all emission observed in the galaxy has been excited by photoionization and do not show any signs of shocks. The points lying over the separation curve in the diagram correspond to the regions of low brightness with low signal-to-noise ratio. Nevertheless, we should note a limited implication of this method of construction of these diagnostic diagrams, because the inhomogeneous reddening may lead to incorrect results. Also the low metallicity should shift the separation line to the area of lower line ratios. But even proposing that all points corresponding to the right wing of the 'seagull shape' in Fig. 15 should lie under the curve, the collision excitation revealed by that way will be important only in the diffuse surrounding of the HSK 45 nebula.

If shock waves from possible SNe and/or stellar winds play an important role in the excitation of emission lines in some regions, we should be able to reveal the corresponding kinematic signatures. In bright nebulae of the eastern chain, where radio observations suggested the presence of supernova remnants, we found no signs of high velocities typical of not too old supernova remnants. However, high-velocity components of the Hα line (in some places having the elevated velocity dispersion) are indeed observed in the outer weakly ionized structures in the SE and NE areas and especially in the N area, where the brightest nebula, HSK 45, is located (see Figs. 7, 8 and 9). We currently can not say firmly whether these high-velocity motions are associated with the inflow of kinetic energy from supernova explosions or from the winds of O type stars. Note, however, that when shock waves from supernovae propagate in an inhomogeneous (cloudy) medium, all typical shock manifestations – via emission, morphology or kinematics, become amorphous (Korolev et al. 2015). Hence, given that the region under study has been a subject of repeated exposure of strong perturbing factors (ionization fronts, wind flows) over long time, the absence of clear signs of supernovae can be explained by the inhomogeneity of the gaseous environment.

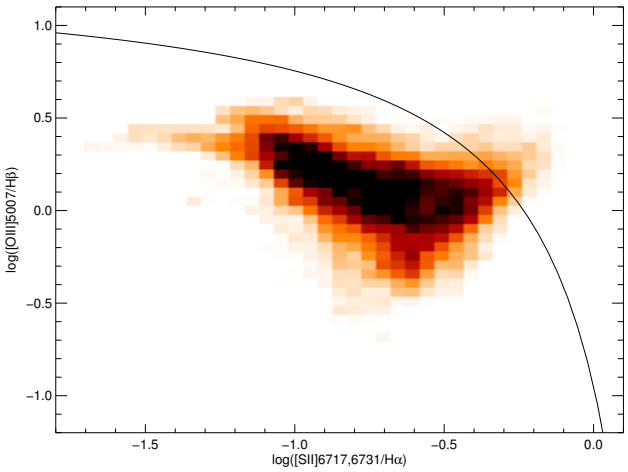

Figure 15. Diagnostic diagram log([O III]5007/Hβ) (computed by dividing the Hα flux by 2.86) vs log([S II]6717, 6731/Hα) constructed for our narrow-band images in Hα, [S II] and [O III] lines. A separation line from Kewley et al. (2001) between regions of pure photoionization excitation and of significant contribution of the shocks is shown by a black line.

7 SUMMARY

A detailed analysis of the structure and kinematics of all bright H II complexes of ongoing star formation in the walls of the supergiant shell of neutral gas in the Ho II galaxy is performed based on the observations carried out at the SAO RAS 6-m telescope with a scanning Fabry–Perot interferometer in the Hα line combined with direct images taken in the Hα, [S II] and [O III] lines. We also used the *HST* archival images. The kinematics of ionized gas is compared to that of neutral gas based on the data of VLA observations in the 21-cm radio line taken from the LITTLE THINGS survey archive (Hunter et al. 2012) and to the stellar population of the area.

The observed data sheds certain light on the process of evolution of giant H I structures under the action by ionizing radiation and inflow of mechanical energy from local bursts of star formation in the walls of these structures.

The following results have been obtained:

(i) We found 22 faint expanding ionized superbubbles in star formation complexes of the galaxy and estimated their expansion velocities and kinematic ages using the results of

the ionized gas kinematics analysis. Also 3 local expanding H I shells tied with star formation complexes in the SGS rim were identified.

(ii) We showed that current star formation episodes in the SGS were more extensive and complex than previously thought: they represent not 'chains' of separate individual bright nebulae in the walls of the H I SGS but rather unified star-forming complexes with sizes of several hundred pc. The formation of such unified complexes is due to the stellar feedback given the strong inhomogeneity of the gas in the SGS walls. Given the large errors of different methods, the inferred age of faint extended and bright more compact structures is consistent with the assumption that they are unified complexes of ongoing star formation.

(iii) We suggest that the last episode of star formation in the galaxy that we observe as areas of bright H II regions and shells in the northern wall of the SGS was triggered by its collision with giant shell-like H I structures located north of the SGS.

(iv) We discovered a faint ionized supershell inside the neutral SGS. The origin of this weak Hα emission somewhat differs from that of the faint inner ionized supershell that we earlier found in the SGS in IC 2574 galaxy, where the leakage of ionizing photons from bright H II regions in the walls of the SGS is proposed as a main ionization source (Egorov et al. 2014). In Ho II, five OB stars located inside the ionized supershell can explain its emission; however, we do not also rule out the leakage of ionizing photons from bright H II regions.

(v) We have not been found any clear kinematic signatures of the effect of shock waves associated with supernova remnants in the eastern chain of bright nebulae earlier suspected of the synchrotron component of the radio emission.

ACKNOWLEDGEMENTS

We are thankful to the anonymous referee for the constructive comments.

This work is based on observations obtained with the 6-m telescope of the Special Astrophysical Observatory of the Russian Academy of Sciences carried out with the financial support of the Ministry of Education and Science of the Russian Federation (agreement No. 14.619.21.0004, project ID RFMEFI61914X0004).

The study was supported by the Russian Foundation for Basic Research (projects 14-02-00027, 15-32-21062, 15-02-08293 and 15-52-45114-IND). The study of gas kinematics was supported by the RSCF grant No. 14-22-00041. YS is also thankful to the Grant of the President of the Russian Federation for Support of the Leading Scientific Schools NSh-4235.2014.2. AVM is also grateful for the financial support via the grant MD3623.2015.2 from the President of the Russian Federation.

This research has made use of the NASA/IPAC Extragalactic Database (NED) which is operated by the Jet Propulsion Laboratory, California Institute of Technology, under contract with the National Aeronautics and Space Administration, and of the Lyon Extragalactic Database (LEDA).

The study is partially based on observations made with the NASA/ESA Hubble Space Telescope, obtained from the Data Archive at the Space Telescope Science Institute, which is operated by the Association of Universities for Research in Astronomy, Inc., under NASA contract NAS 5-26555. These observations are associated with programs # 10522 and # 10605.

REFERENCES

Abramova O. V., Zasov A. V., 2012, Astron.Letters, 38, 755
Afanasiev V.L., Moiseev A.V., 2011, Baltic Astronomy, 20, 363
Bagetakos I., Brinks E., Walter F., de Blok W.J.G., Usero A., Leroy A.K., Rich J.W., Kennicutt R.C., 2011, AJ, 141, 2011
Banerjee A., Jog C.J., Brinks E., Bagetakos I., 2011, MNRAS, 415, 687
Bastian N. et al., 2011, MNRAS, 412, 1539
Bernard E.J., Ferguson A. M. N., Barker M.K., Irwin M.J., Jablonka P., Arimoto N., 2012, MNRAS, 426, 3490
Bigiel F., Leroy A., Walter F., Brinks E., de Blok W. J. G., Madore B., Thornley M. D., 2008, AJ, 136, 2846
Bigiel F., Leroy A., Walter F., Blitz L., Brinks E., de Blok W. J. G., Madore B. , 2010, AJ, 140, 1194
Boomsma R., Oosterloo T.A., Fraternali F., van der Hulst J., Sancisi R. , 2008, A&A, 490, 555
Braun, R., Oosterloo, T. A., Morganti, R., Klein, U., Beck, R., 2007, AAp, 461, 455
Bureau M., Carignan C., 2002, AJ, 123, 1316
Camps-Farinã A., Zaragoza-Cardiel J., Beckman J.E. , Font J., García-Lorenzo B., Erroz-Ferrer S., Amram P., 2015, MNRAS, 447, 3840
Cannon J. M. et al. 2011a, ApJ, 735, 35C
Cannon J. M. et al. 2011b, ApJ, 735, 36C
Chernin A.D., Efremov, Yu.N., Voinovich, P.A., 1995, MNRAS, 275, 313
Chevalier R.A., 1974, ApJ, 188, 501
Cox D. P., 1972, ApJ, 178, 159
Dalcanton J.J. et al., 2008 ApJS, 183, 67
Dicaire I. et al., 2008 MNRAS, 385, 553
Dib S., Burkert A. 2005, ApJ, 630, 238
Draine, B. T., 2011, Physics of the Interstellar and Intergalactic Meduim. Princeton
Efremov, Yu.N., Afanasiev V.L., Egorov O.V., 2011, Astron.Bull., 66, 304
Egorov O.V., Lozinskaya T.A., Moiseev A.V., 2010, Astron.Rep., 54, 277
Egorov O.V., Lozinskaya T.A., Moiseev A.V., 2013, MNRAS, 429, 1450
Egorov O.V., Lozinskaya T.A., Moiseev A.V., Smirnov-Pinchukov G.V., 2014, MNRAS, 444, 376
Egorov O.V., Lozinskaya T.A., Moiseev A.V., 2015, Astron.Astrophys.Trans., 29, 17
Egorov O.V., Lozinskaya T.A., Moiseev A.V., 2016, MNRAS, submitted
Elmegreen B. G. 1997, ApJ, 477, 196
Elmegreen B. G., Chiang, W.-H., 1982, ApJ, 253, 666
Heald G., Braun R., Edmonds R., 2009, A&A, 503, 409
Henney, W. J., Arthur, S. J., Williams, R. J. R., Ferland, G. J., 2005, ApJ, 621, 328
Henney, 2007, in Hartquist T.W., Pittard J. M., Falle. S. A. E. G. eds., Astrophys. & Space Sci. Proc., 1, Diffuse Matter from Star Forming Regions to Active Galaxies, Springer, Dordrecht, p.103
Hodge P., Strobel N.V., Kennicutt R.C., PASP, 1994, 106, 309
Hong S., Calzetti D., Gallagher J.S., Martin C.L., Conselice C.J., Pellerin A., 2013, ApJ, 777, 63
Hunter D.A., Hawley W.N., Gallagher J.S., 1993, AJ, 106, 1797
Hunter D.A. et al., 2012, AJ, 144, 134

Hunter D.A., Elmegreen B.G., Gehret E., 2016, AJ, 151, 136
Karachentsev I.D., Kaisin S.S., 2007, AJ, 133, 1883
Karachentsev I.D., Makarov D.I., Kaisina E.I., 2013, AJ, 145, 101
Kennicutt R.C. Jr. et al., 2003, PASP, 115, 928
Kennicutt R.C. et al., 2011, PASP, 123, 1347
Kewley L. J., Dopita M. A., Sutherland R. S., Heisler C. A., Trevena J., 2001, ApJ, 556, 121
Kim S., Dopita M. A., Stavelet-Smith L., Bessel M., 1999, A&A, 350, 230
Korolev V.V., Vasiliev E.O., Kovalenko I.G., Shchekinov Yu.A., 2015, ARep, 59, 690
Lada C.J., Lada E.A., ARA&A, 41, 57, 2003.
Lehmann I et al., 2005, A&A, 431, 847
Leitherer C. et al., 1999, ApJ, 123, 3
Leroy A.K. et al., 2009, AJ, 137, 4670
Lozinskaya T.A., 2002, Astron. Astroph. Transactions, 21, 223
Lozinskaya T.A., Moiseev A.V., Podorvanyuk N.Yu., 2003, RMXAA, 15, 284
Markova N. & Puls J., 2008, A&A, 478, 823
Martins F., Schaerer D., Hilliier D.J., 2005, A&A, 436, 1049
Maschenko S.Ya., Silich S.A., 1995, Astron.Rep., 39, 587
McCray R., Kafatos M., 1987, ApJ, 317, 190
McQuinn K.B.W., Skillman E.D., Cannon J.M., Dalcanton J. J., Dolphin A., Stark D., Weisz D., 2009, ApJ, 695, 561
McQuinn K.B.W. et al., 2010a, ApJ, 721, 297
McQuinn K.B.W. et al., 2010b, ApJ, 724, 49
Moiseev A.V., 2002, Bull. Spec. Astrophys. Obs., 54, 74
Moiseev A.V., Egorov O.V., 2008, Astrophysical Bulletin, 63, 181
Moiseev A.V., Lozinskaya T.A., 2012, MNRAS, 423, 1831
Moiseev A.V., 2014, Astrophysical Bulletin, 69, 1
Moiseev A.V., 2015, Astrophysical Bulletin, 70, 494
Moustakas J., Kennicutt R.C. Jr., Tremonti C.A., Dale D.A., Smith J.-D. T., Calzetti D., 2010, ApJS, 190, 233
Muñoz-Tuñón C., Tenorio-Tagle G., Castañeda H.O., Terlevich R., 1996, AJ, 112, 1636
Nath, B.B. & Shchekinov, Yu., 2013, ApJL, 777, L12
Oh S.-H., de Blok W. J. G., Brinks E., Walter F., Kennicutt R. C. Jr., 2011, AJ, 141, 193
Ott J., Walter F., Brinks E., Van Dyk S. D., Dirsch B., Klein U., 2001, AJ, 122, 3070
O'Connell R.W., 1997, AIP Conf. Proc., 408, 11
Osterbrock D.E, Ferland G.J., 2006, Astrophysics of Gaseous Nebulae and Active Galactic Nuclei, 2nd Edition. Univ. Sci. Books
Pellegrini E.W., Oey M.S, Winkler P.F., Smith R.C., Points S., 2011, Bull. Soc. R. Sci. de Liége, 80, 410
Puche D., Westpfahl D., Brinks E., Roy J.-R., 1992, AJ, 103, 184
Relaño M., Beckman J. E., 2005, A&A, 430, 911
Rhode K. L., Salzer J. J., Westpfahl D., Radice L. A. 1999, AJ, 118, 323
Sánchez-Salcedo F.J., Hidalgo-Gámez A.M., Martínez-García E.E., 2014, Rev.Mex, 50, 225
Sánchez-Cruces M., Rosado M., Rodríguez-González A., Reyes-Iturbide J., 2015, ApJ, 799, 231
Schaerer D., Vacca W. D., 1998, ApJ, 497, 618
Sharma P., Roy A., Nath B.B., Shchekinov Yu., 2014, MNRAS, 443, 3463
Shi Y., Armus L. Helou G., Stierwalt S., Gao Y. Wang J., Zhang Z., Gu Q., 2014, Nature, 514, 335
Simpson C.E., Hunter D.A., Knezek P.M., 2005, AJ, 129, 160
Silich S., Lozinskaya T., Moiseev A., Podorvanyuk N., Rosado M., Borissova J., Valdez-Gutiérrez M., 2006, A&A, 448, 123
Stasińska G., Leitherer C., 1996, ApJS, 107, 661
Stewart S.G. et al., 2000, ApJ, 529, 201
Tenorio-Tagle G., 1979, A&A, 71, 59
Tenorio-Tagle G., 1981, A&A, 94, 338
Tenorio-Tagle G., Bodenheimer P. 1988, ARA&A, 26, 145
Tomisaka, K., Habe, A., Ikeuchi, S., 1981, Ap&SS, 78, 273
Tomita A., Ohta K., Nakanishi K., Takeuchi T.T., Saito M., 1998, AJ, 116, 131
Tongue T.D., Westpfahl D.J., 1995, AJ, 109, 2462
Vasiliev E. O., Nath, B. B., Shchekinov, Yu. A., 2015, MNRAS, 446, 1703
Vorobyov E. I., Shchekinov Y. A. 2004, A&A, 416, 499
Wada K., Spaans M., Kim S., 2000, ApJ, 540, 797
Walter F., 2007, ApJ, 661, 102
Walter F., Brinks E., de Blok W. J. G., Bigiel F., Kennicutt R. C. Jr, Thornley M.D., Leroy A., 2008, AJ, 136, 2563
Warren S.R. et al., 2011, ApJ, 738, 10
Weaver R., McCray R., Castor J., Shapiro P., Moore R., 1977, ApJ, 218, 377
Weisz D. R., Skillman E. D., Cannon J. M., Dolphin A. E., Kennicutt R. C., Lee J., Walter F., 2008, ApJ, 689, 160
Weisz D. R., Skillman E. D., Cannon J. M., Dolphin A. E., Kennicutt R. C., Lee J., Walter F. 2009a, ApJ, 704, 1538
Weisz D.R., Skillman E.D., Cannon J.M., Walter F., Brinks E., Ott J., Dolphin A.E., 2009b, ApJ, 691, L59
Wiebe D.S., Khramtsova M.S., Egorov O.V., Lozinskaya T.A., 2014, Astron. Letters, 40, 278
Yadav N. Mukherjee D., Sharma P., Nath B. arxiv:1603.00815
Young L. M., Lo K. Y. 1997, ApJ, 490, 710
Zasov A. V., Abramova O. V., Astron Astroph Trans, 2012, 27, 351